Viscoelasticity in Electro Active Polymers

S.M. Khosrownejad

Report/Preprint No. 11–I–04
Institut für Mechanik (Bauwesen) · Lehrstuhl I · Prof. C. Miehe
Universität Stuttgart, 70550 Stuttgart, Pfaffenwaldring 7, Germany

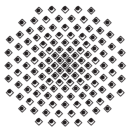

Contents

1. Introduction to Electro Active Polymers(EAPs).
- 1.1. State of the Art.
- 1.2. Structure of the Thesis.

2. Introduction to Continuum Electromechanics at Finite Strains.
- 2.1. Geometrical Aspects of Finite Deformation Kinematics.
- 2.2. Fundamental Stress Measures.
- 2.3. Maxwell's Laws for Electrostatics.
- 2.4. Extended Balance Laws of Continuum Thermodynamics.
- 2.5. Fully-Coupled Boundary Value Problems.

3. Finite Electro-Elasticity.
- 3.1. Thermodynamically-Consistent Constitutive Theory.
- 3.2. Enthropy Inequality.
- 3.3. Elastic Material Response Formulation.
- 3.4. Electrical Material Response Formulation.

4. Finite Electro Visco Elasticity.
- 4.1. Free Mixed Energy Enthalpy Function for Viscoelasticity.
- 4.2. Evolution Equation .
- 4.3. Time Integration Algorithm.

5. Numerical Implementation of Finite Electromechanics.
- 5.1. Electro-Mechanical Boundary Value Problem.
- 5.2. Continuus Variational Formulation.
- 5.3. Finite Element Discretization.

6. Numerical Results.
- 6.1. Basic Tests.
- 6.2. Selected Boundary Value Problems.

Acknowledgement

This thesis was conducted at the Institut für Mechanik (Bauwesen), Lehrstuhl I, Universität Stuttgart as part of the curriculum of the *Erasmus Mundus Master of Science in Computational Mechanics*, a joint initiative of the Universitat Politècnica de Catalunya (Barcelona, Spain), Swansea University (UK), Ecole Centrale Nantes (France) and the Universität Stuttgart (Germany) in cooperation with the *International Center for Numerical Methods in Engineering* (CIMNE).

I am grateful to Prof. Dr.-Ing. Christian Miehe for allowing me this opportunity and for his guidance. I would like to extend my heartfelt gratitude to my supervisor Dr.-Ing. Daniele Rosato from whom I have learnt a great deal not only in the topics covered in this theis but also from an overall perspective in research.

I am greatly indebted to my family specially to my wife who have been constant source of encouragment throughout my studies. Last but not least, I would also like to take this opportunity to thank the European Commission for the Erasmus Mundus Program which funded me throughout the two years course without which it would never have been possible to work with eminent faculty and a rich research environment.

1. Introduction to Electro Active Polymers(EAPs)

Fundamental and technological interest in *Electro Active Polymers* (EAPs), representing a broad class of organic actuators that exhibit large dimensional changes upon electrical stimulation, has grown tremendously over the past decade. Electro Active polymers can best be described as soft, flexible materials that are capable of converting electrical energy to mechanical energy and thus producing a force and/or motion.

EAPs can be broadly classified as *electronic* or *ionic* according to their operational mechanism. Electronic EAPs generally exhibit superior performance relative to ionic EAPs in terms of actuation strain and are in the focus of this research. The electronic EAPs, commonly distinguished on the basis of their actuation mechanism as either *electrostrictive (ferroelectric polymers)* or *electrostatic (dielectric elastomers)*(Shankar et al. [22])(Plante and Dubowsky et al. [18]).

Ferroelectric polymers have a *non-centro-symmetric structure that exhibits permanent electric polarization*. These materials possess dipoles that can be aligned in an electric field and maintain their polarization. The induced polarization can be removed by applying a reverse electric field or by heating above the material's Curie temperature. They exhibit nonlinear polarization curves demonstrating pronounced hysteresis. The polymers exhibiting these properties are limited mainly to poly(vinylidene difluoride)(PVDF), some PVDF copolymers, certain odd-numbered polyamides such as Nylon 7 and Nylon 11 and blends thereof [3].

On the other side Dielectric Elastomer actuators does not have any intrinsic electromechanical coupling. They are essentially compliant variable capacitors. They consist of a thin elastomeric film coated on both sides with compliant electrodes. When an electric field is applied across the electrodes, the electrostatic attraction between the opposite charges on opposing electrode and the repulsion of the like charges on each electrode generate stress on the film causing it to contract in thickness and expand in area. Figure 1 shows the the activation mechanisms of these two main types of Electronic EAPs and their differences. Most elastomers used are essentially incompressible, so any decrease in thickness results in a concomitant increase in the planar area. The area expansion can be readily measured if the films are subjected to tensile prestrain: the non-active areas in tension surrounding the active area pulls the expanded active area and keeps it flat.

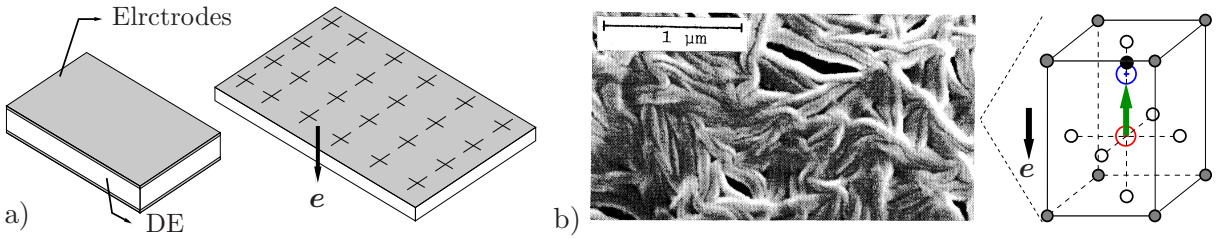

Figure 1: Electronic Electro Active Polymers are divided two two main classes. In *Dielectric Elastomers*(a) a passive elastomer film is sandwiched between two compliant electrodes. Electromechanical effect is a result of maxwell stresses that is not an intrinsic material property. *Ferroelectric Polymers* (b) have intrinsic elecromechanical coupling properties and are able to maintain a permanent electric polarization that can be reversed or switched, in an external electric field.

1.1. State of the Art

The constitutive modeling of electro-mechanical materials has been of the interest of several researchers since 1950's. Among others Rosato [21] provided a finite strain electromechanical formulation and appropriate finite element formulation which have been used in this work.

Finite viscoelastic over-stress response becomes apparent in creep and relaxation tests as well as in cyclic loading processes. This phenomena has been shown to be important in the modeling of DEs [20, 26]. Lubliner's work [12] was one of the first attempts to develop a large strain viscoelastic model. He split the free energy of a viscoelastic solid in two parts : the first part describing the rate-independent material behavior and the second incorporating time-dependent effects. He further assumed a multiplicative decomposition of the deformation gradient into elastic and inelastic parts. An important point in developing models of this form is the choice of the evolution equation for the internal variables. In the theory of linear viscoelasticity, which is only valid for small deformations and small perturbations away from thermodynamic equilibrium, one can take either the "over-stress" or the inelastic strain as an internal variable. Due to the fact that the relationship between these two is linear and additionally all stress and strain measures coincide for small deformations, the structure of the evolution equation is evident. Simo [23] and Holzapfel [8] the same "over-stress" approach to develop the model. Our approach will be similar to what these researchers done and we will extend their formulation for coupled electro-mechanical materials. However there are other authors who used othe approaches like multiplicative decomposition of the deformation gradient into elastic and inelastic parts (see e.g. Reese & Govindjee [6]) or metric based evolution equations (Miehe & Keck [15]).

1.2. Structure of the Thesis

The aim of this work is to study viscoelastic behavior of Electro Active Polymers and in particular Dielectric Elastomers in a finite strain context. We present here finite elasticity and finite viscoelasticity of these materials. The free energy functions that are presented are motivated by the the experimental results and are consistent with mathematical theory of material modeling.

In the second chapter, an introduction to continuum electro mechanics is provided. Here, apart from the standard finite deformation equations, we introduce the electric field variables and their mapping properties along along with the balance principles of continuum electromechanics. We then go on to describe a thermodynamically consistent constitutive theory and proceed to show, how we can solve such coupled boundary value problems, within in a variational framework.

The third chapter presents material modeling basics in finite electro elasticity. Here, we will also propose appropriate material model for Dielectric Elastomers. The solution of the balance equations in combination with the constitutive equations gives us the electro-mechanical fields within the region under consideration.

In the forth chapter, we will present the viscoelastic material modeling at large strain. This derivation includes the the typical steps of defining the finite deformation viscoelasticity. We will start with free energy function which is established in the previous chapter for elasticity and extend it for viscoelastic case. Rate equation as well as numerical treat-

ment will be covered.

The fifth chapter, presents an alternative compact finite element formulation used to solve the boundary value problems. This is the formulation that has been used in obtaining the numerical results that have been presented in the penultimate section of the thesis.

The sixth chapter reports the numerical results. we presented here several material point level tests as well as two dimensional and three dimensional boundary value problems which have been tested to show the reliability of the formulation.

2. Introduction to Continuum Electromechanics at Finite Strains

In this chapter the continuum-thermodynamics basis for a finite deformation theory with an extension to electrostatics is established. This derivation includes the typical steps of defining the finite deformation kinematics based on fundamental geometric mappings, of introducing stress measures, the basics of electrostatics as well as the global and local balance laws of continuum electromechanics.

The following description of finite deformation kinematics conceptually relies on the terminology of modern differential geometry (cf. Marsden & Hughes [13]).

2.1. Geometrical Aspects of Finite Deformation Kinematics

A *material body* B is mathematically defined as the open set of material points P, which can be identified with geometrical points in the three-dimensional Euclidean space $\mathbb{R}^3$ via the one-to-one *configuration placement map* $\boldsymbol{\chi}$. The *motion* of a body is the time-parameterized family of configurations

$$\boldsymbol{\chi}_t := \begin{cases} B \to \mathcal{B}_t \in \mathbb{R}^3 \ , \\ P \in B \mapsto \boldsymbol{x}_t = \boldsymbol{\chi}_t(P) \in \mathcal{B}_t \ . \end{cases} \tag{1}$$

This relation therefore describes the configuration of the body B in $\mathbb{R}^3$ at time t. In the *referential description of motion* one defines the *reference* or *Lagrangian configuration* as the placement of the body at time t_0, i.e. $\mathcal{B} := \boldsymbol{\chi}_{t_0}(B)$, with the *reference coordinates* $\boldsymbol{X} := \boldsymbol{\chi}_{t_0}(P) \in \mathcal{B}$. The *current* or *Eulerian configuration* at time t is defined as $\mathcal{S} := \boldsymbol{\chi}_t(B)$, with the *spatial coordinates* $\boldsymbol{x} := \boldsymbol{\chi}_t(P) \in \mathcal{S}$. The motion of the body with respect to the

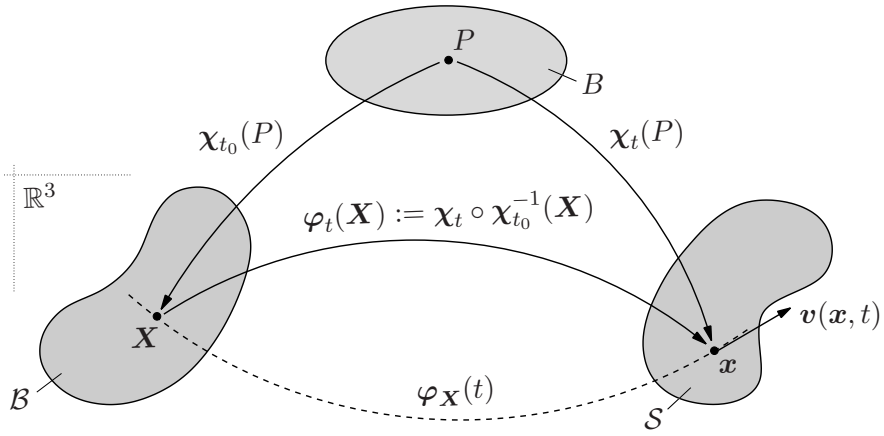

Figure 2: Identification of the position $\boldsymbol{X} \in \mathcal{B}$ of a particle $\boldsymbol{P} \in B$ in three-dimensional Euclidian space $\mathbb{R}^3$ through the configuration map $\boldsymbol{\chi}_t$ and description of the motion of a material point w.r.t the reference configuration via the deformation map $\boldsymbol{\varphi}_t$.

reference configuration is then defined by the nonlinear *deformation map*

$$\boldsymbol{\varphi} := \begin{cases} \mathcal{B} \times \mathbb{R}_+ \to \mathcal{S} \in \mathbb{R}^3 \ , \\ (\boldsymbol{X}, t) \mapsto \boldsymbol{x} = \boldsymbol{\varphi}(\boldsymbol{X}, t) = \boldsymbol{\varphi}_t(\boldsymbol{X}) \ , \end{cases} \tag{2}$$

which maps the material points $\boldsymbol{X} \in \mathcal{B}$ onto their deformed spatial positions $\boldsymbol{x} \in \mathcal{S}$ as shown in Figure 2.

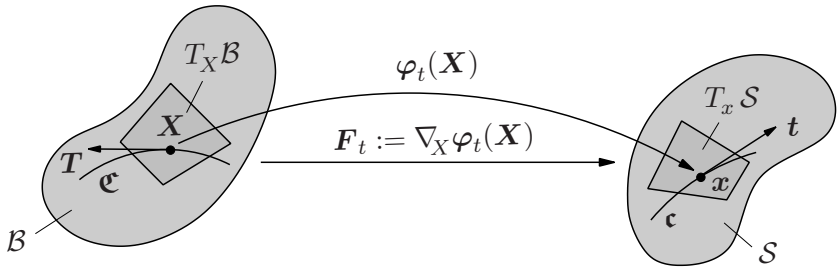

Figure 3: The deformation gradient acting as the linear tangent map, which transforms the material vector $\boldsymbol{T} \in T_X\mathcal{B}$, tangent to a material curve $\mathfrak{C}$ at $\boldsymbol{X}$, onto the associated spatial vector $\boldsymbol{t} \in T_x\,\mathcal{S}$, tangent to the material curve $\mathfrak{c}$ at $\boldsymbol{x}$.

Mathematically, the *deformation gradient* $\boldsymbol{F}$ is defined as the Fréchet derivative of the deformation map, i.e. $\boldsymbol{F}_t(\boldsymbol{X}) := \operatorname{Grad} \boldsymbol{\varphi}_t$. Geometrically, the deformation gradient can be interpreted as the *linear tangent map* which maps tangents $\boldsymbol{T}$ to material curves, i.e. elements of the tangent spaces $T_X\mathcal{B}$ of the manifold $\mathcal{B}$, onto tangents $\boldsymbol{t}$ of the deformed material curves, i.e. elements of the tangent space $T_x\,\mathcal{S}$ of the manifold $\mathcal{S}$, according to

$$\boldsymbol{F}_t := \begin{cases} T_X\mathcal{B} \to T_x\,\mathcal{S} \ , \\ \boldsymbol{T} \mapsto \boldsymbol{t} = \boldsymbol{F}_t\boldsymbol{T} \ , \end{cases} \tag{3}$$

as visualized in Figure 3. Note that, since $\boldsymbol{\varphi}_t$ is a one-to-one mapping and must prohibit material interpenetration, the deformation gradient is subject to the following constraints $J := \det \boldsymbol{F} > 0$. The determinant of the deformation gradient can further directly be interpreted as another fundamental mapping, the *volume map*, which relates infinitesimal reference volume elements dv to their deformed spatial counterparts dV via the relation

$$J = \det \boldsymbol{F} := \begin{cases} \mathbb{R}_+ \to \mathbb{R}_+ \ , \\ dV \mapsto dv = \det \boldsymbol{F}\, dV \ . \end{cases} \tag{4}$$

The *co-factor* of the deformation gradient $\operatorname{cof} \boldsymbol{F}$ is defined as the derivative of the volume map with respect to $\boldsymbol{F}$. It can geometrically be interpreted as the *area map*, which maps infinitesimal reference area elements onto the associated spatial ones via the relation $\boldsymbol{n}\, da = J\boldsymbol{F}^{-T}\boldsymbol{N}\, dA = (\operatorname{cof} \boldsymbol{F})\boldsymbol{N}\, dA$, also known as *Nanson's formula*. Moreover, $\boldsymbol{F}^{-T}$ can thus be identified as the *normal map*, that maps normals of material surfaces, or, again from the differential geometry view point, elements of the co-tangent space $T_X^*\mathcal{B}$, onto normals of the deformed spatial surfaces, i.e. elements of the co-tangent space $T_x^*\mathcal{S}$, according to

$$\boldsymbol{F}^{-T} := \begin{cases} T_X^*\mathcal{B} \to T_x^*\mathcal{S} \ , \\ \boldsymbol{N} \mapsto \boldsymbol{n} = \boldsymbol{F}^{-T}\boldsymbol{N} \ . \end{cases} \tag{5}$$

For the specification of coordinate representations one introduces the Cartesian frames $\{\boldsymbol{E}_i\}$ for $T_X\mathcal{B}$, $\{\boldsymbol{E}^i\}$ for $T_X^*\mathcal{B}$, $\{\boldsymbol{e}_i\}$ for $T_x\,\mathcal{S}$ and $\{\boldsymbol{e}^i\}$ for $T_x^*\mathcal{S}$. Capital letter indices $i = \{A, B, C\}$ are used for Lagrangian and lower case indices $i = \{a, b, c\}$ for Eulerian settings.[1] The reference and spatial coordinates are thus expressed as $\boldsymbol{X} = X^A\boldsymbol{E}_A$ and

[1]Note that these frames will typically coincide, but they have formally been considered here for the sake of clarity.

$\boldsymbol{x} = x^a \boldsymbol{e}_a$. The deformation gradient then admits the representation $\boldsymbol{F} = F^a{}_A \boldsymbol{e}_a \otimes \boldsymbol{E}^A$, with $F^a{}_A = \partial\varphi^a/\partial X^A$. Likewise, the component forms of the mappings (3) and (5) read $t^a = F^a{}_A T^A$ and $n_a = (F^{-1})^A{}_a N_A$.

In order to be able to measure geometric quantities such as the length of vectors, however, one must additionally introduce *metric tensors*. In global Cartesian frames the *covariant* and *contravariant Lagrangian metric tensors* admit the reduced representation $\boldsymbol{G} = \delta_{AB}\boldsymbol{E}^A \otimes \boldsymbol{E}^B$ and $\boldsymbol{G}^{-1} = \delta^{AB}\boldsymbol{E}_A \otimes \boldsymbol{E}_B$, where δ_{AB} and δ^{AB} are Kronecker deltas. Similarly, the *covariant* and *contravariant Eulerian metric tensors* reduce to $\boldsymbol{g} = \delta_{ab}\boldsymbol{e}^a \otimes \boldsymbol{e}^b$ and $\boldsymbol{g}^{-1} = \delta^{ab}\boldsymbol{e}_a \otimes \boldsymbol{e}_b$, respectively. The metric tensors represent mappings of vectors, i.e. elements of the tangent spaces, onto normals (co-vectors), i.e. elements of the co-tangent spaces. For the Lagrangian and the Eulerian manifolds these mappings are defined by

$$\boldsymbol{G} := \begin{cases} T_X\mathcal{B} \to T_X^*\mathcal{B} \ , \\ \boldsymbol{T} \mapsto \boldsymbol{N} = \boldsymbol{G}\boldsymbol{T} \ , \end{cases} \qquad \boldsymbol{g} := \begin{cases} T_x\,\mathcal{S} \to T_x^*\mathcal{S} \ , \\ \boldsymbol{t} \mapsto \boldsymbol{n} = \boldsymbol{g}\boldsymbol{t} \ . \end{cases} \tag{6}$$

These mappings can also be interpreted as *index lowering* or *raising procedures* since the coordinate representations of (6) read $N_A = G_{AB}T^B = \delta_{AB}T^B$ and $n_a = g_{ab}t^b = \delta_{ab}t^b$, respectively. It is

Commutative diagrams, such as the ones displayed in Figure 4, significantly facilitate the geometric meaning of the introduced mappings. Based on the definitions of the

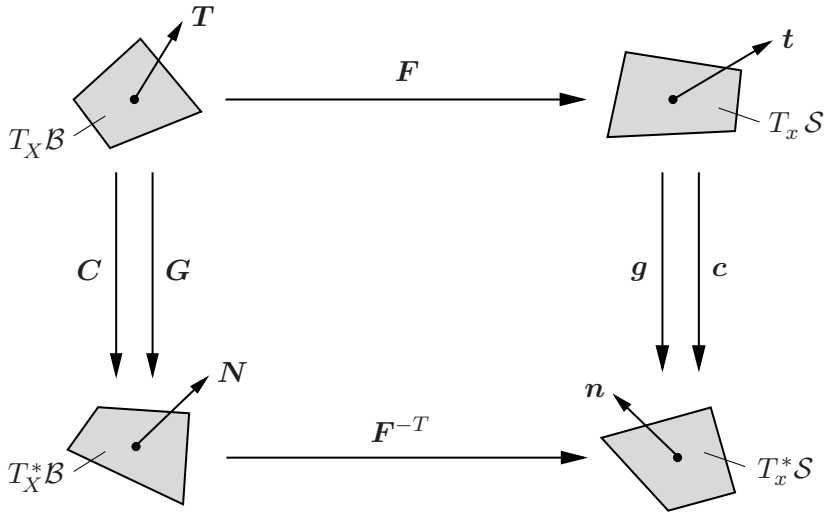

Figure 4: Commutative diagram illustrating the *'push-forward'* and *'pull-back'* of the covariant reference metric $\boldsymbol{G}$ and spatial metric $\boldsymbol{g}$.

mappings (3), (5), (6) and their respective inverse mappings, one can introduce additional deformation measures. The *right Cauchy-Green tensor* $\boldsymbol{C}$ can in this context be defined as the *'pull-back'* of the spatial metric

$$\boldsymbol{C} := \boldsymbol{\varphi}^*(\boldsymbol{g}) = \boldsymbol{F}^T\boldsymbol{g}\boldsymbol{F} \ , \qquad \text{or} \qquad C_{AB} = F^a{}_A g_{ab} F^b{}_B \ , \tag{7}$$

in coordinate representation, and can thus be interpreted as the 'representation of the current metric in the Lagrangian setting' or 'convected spatial metric'. Similarly, the *inverse right Cauchy-Green tensor* $\boldsymbol{C}^{-1}$ is defined as

$$\boldsymbol{C}^{-1} := \boldsymbol{\varphi}^*(\boldsymbol{g}^{-1}) = \boldsymbol{F}^{-1}\boldsymbol{g}^{-1}\boldsymbol{F}^{-T} \ , \qquad \text{or} \qquad \big(C^{-1}\big)^{AB} = \big(F^{-1}\big)^A{}_a g^{ab} \big(F^{-1}\big)^B{}_b \ . \tag{8}$$

Accordingly, via appropriate *'push-forward'* operations, one defines the *left Cauchy-Green tensor* $\boldsymbol{b}^f$, often called the *Finger tensor*, and the *inverse left Cauchy-Green tensor* $\boldsymbol{c}$, respectively, as

$$\boldsymbol{b}^f := \boldsymbol{\varphi}_* \left(\boldsymbol{G}^{-1}\right) = \boldsymbol{F}\boldsymbol{G}^{-1}\boldsymbol{F}^T \ , \qquad \text{or} \qquad b^{ab} = F^a{}_A G^{AB} F^b{}_B \ , \tag{9}$$

$$\boldsymbol{c} = \left(\boldsymbol{b}^f\right)^{-1} := \boldsymbol{\varphi}_* \left(\boldsymbol{G}\right) = \boldsymbol{F}^{-T}\boldsymbol{G}\boldsymbol{F}^{-1} \ , \qquad \text{or} \qquad c_{ab} = \left(F^{-1}\right)^A{}_a G_{AB} \left(F^{-1}\right)^B{}_b \ . \tag{10}$$

The reader is again referred to Figure 4 for a graphical representation of the geometrical mapping properties of the introduced metric tensors.

2.2. Fundamental Stress Measures

Consider an arbitrary *part* $\mathcal{P} \subset \mathcal{B}$ cut out of the undeformed body in the reference configuration and its deformed counterpart $\mathcal{P}_t \subset \mathcal{S}$ with the respective closed surfaces $\partial\mathcal{P}$ and $\partial\mathcal{P}_t$, as shown in Figure 5. In the current configuration one replaces the mechanical action of the rest of the body on the cut-out part by the spatial traction field $\boldsymbol{t}$. According

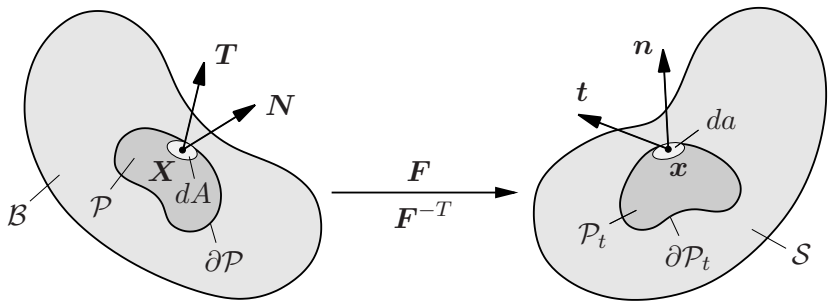

Figure 5: The material and spatial traction vectors $\boldsymbol{T}(\boldsymbol{X}, t; \boldsymbol{N}) \in T_X\mathcal{B}$ and $\boldsymbol{t}(\boldsymbol{x}, t; \boldsymbol{n}) \in T_x\mathcal{S}$ representing the forces per unit area exerted by the cut-off remainder of the body on the surfaces $\partial\mathcal{P}$ and $\partial\mathcal{P}_t$ of the cut-out parts in the material and spatial settings, respectively.

to *Cauchy's theorem*, $\boldsymbol{t}$ is assumed to be a linear function of the orientation of the cut, represented by the spatial unit normal $\boldsymbol{n} \in T_x^*\mathcal{S}$ to the surface $\partial\mathcal{P}_t$, or specifically

$$\boldsymbol{t}(\boldsymbol{x}, t; \boldsymbol{n}) := \boldsymbol{\sigma}(\boldsymbol{x}, t)\boldsymbol{n} \ , \qquad \text{or} \qquad t^a = \sigma^{ab} n_b \ . \tag{11}$$

Therein $\boldsymbol{\sigma}$ is the *Cauchy stress tensor*, which in our considered geometrical framework can be understood as a contravariant mapping of the form

$$\boldsymbol{\sigma} := \begin{cases} T_x^*\mathcal{S} \to T_x\mathcal{S} \ , \\ \boldsymbol{n} \mapsto \boldsymbol{t} = \boldsymbol{\sigma}\boldsymbol{n} \ . \end{cases} \tag{12}$$

Another common spatial stress measure is the *Kirchhoff stress tensor*, or *weighted Cauchy stress tensor*, $\boldsymbol{\tau} := J\boldsymbol{\sigma}$, which, due to the scalar nature of J, preserves the geometric mapping properties of $\boldsymbol{\sigma}$.

One can further introduce a scaled spatial traction vector $\tilde{\boldsymbol{t}} \in T_x\mathcal{S}$ that produces a resultant force on an element of the reference surface which is equal to the force exerted by $\boldsymbol{t}$ on an element of the deformed surface, such that $\boldsymbol{t}\, da = \tilde{\boldsymbol{t}}\, dA$. The *nominal* or *first Piola-Kirchhoff stress tensor* $\boldsymbol{P}$ is then defined via the Cauchy-theorem-type relation

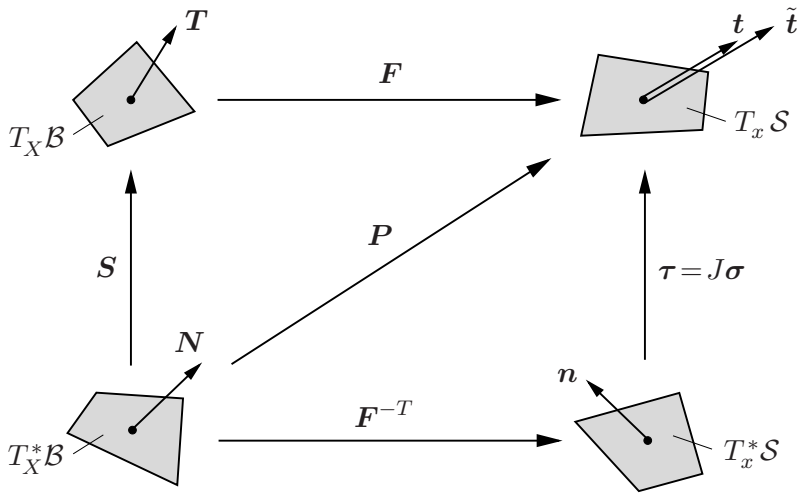

Figure 6: Commutative diagram illustrating the geometric mapping properties of the introduced stress tensors.

$\tilde{\boldsymbol{t}} := \boldsymbol{P}\boldsymbol{N}$, or $\tilde{t}^a = P^{aA}N_A$. Additionally, using Nanson's formula, one obtains the following relation between the introduced stress tensors $\boldsymbol{P} = J\boldsymbol{\sigma}\boldsymbol{F}^{-T} = \boldsymbol{\tau}\boldsymbol{F}^{-T}$. Note that $\boldsymbol{P}$ is a two-point (mixed-variant) tensor possessing the geometrical mapping properties

$$\boldsymbol{P} := \begin{cases} T^*_X\mathcal{B} \to T_x\,\mathcal{S}\ , \\ \boldsymbol{N} \mapsto \tilde{\boldsymbol{t}} = \boldsymbol{P}\boldsymbol{N}\ . \end{cases} \tag{13}$$

The Lagrangian traction vector $\boldsymbol{T} \in T_X\mathcal{B}$ may be defined as the *'pull-back'* of the spatial traction field $\tilde{\boldsymbol{t}} \in T_x\,\mathcal{S}$, i.e. $\boldsymbol{T} = \boldsymbol{\varphi}^*\left(\tilde{\boldsymbol{t}}\right) = \boldsymbol{F}^{-1}\boldsymbol{T}$ as displayed in Figure 5. The *second Piola-Kirchhoff stress tensor* $\boldsymbol{S}$ is then defined via the relation $\boldsymbol{T} := \boldsymbol{S}\boldsymbol{N}$, or $T^A = S^{AB}N_B$, and has the mapping properties

$$\boldsymbol{S} := \begin{cases} T^*_X\mathcal{B} \to T_X\mathcal{B}\ , \\ \boldsymbol{N} \mapsto \boldsymbol{T} = \boldsymbol{S}\boldsymbol{N}\ . \end{cases} \tag{14}$$

The commutative diagram of Figure 6 depicts the geometrical relations between the introduced stress tensors. It is immediately apparent that the following *'pull-back'* operations on the mixed-variant and spatial stress tensors hold.

$$\boldsymbol{S} := \boldsymbol{\varphi}^*\left(\boldsymbol{P}\right) = \boldsymbol{F}^{-1}\boldsymbol{P}\ , \qquad \text{or} \qquad S^{AB} = \left(F^{-1}\right)^A{}_a P^{aB}\ , \tag{15}$$

$$\boldsymbol{S} := \boldsymbol{\varphi}^*\left(\boldsymbol{\tau}\right) = \boldsymbol{F}^{-1}\boldsymbol{\tau}\boldsymbol{F}^{-T}\ , \qquad \text{or} \qquad S^{AB} = \left(F^{-1}\right)^A{}_a \tau^{ab}\left(F^{-1}\right)^B{}_b\ . \tag{16}$$

Accordingly, the converse *'push-forward'* relations of the mixed-variant and reference stress tensors are given by

$$\boldsymbol{\tau} = J\boldsymbol{\sigma} := \boldsymbol{\varphi}_*\left(\boldsymbol{P}\right) = \boldsymbol{P}\boldsymbol{F}^T\ , \qquad \text{or} \qquad \tau^{ab} = P^{aA}F^b{}_A\ , \tag{17}$$

$$\boldsymbol{\tau} := \boldsymbol{\varphi}_*\left(\boldsymbol{S}\right) = \boldsymbol{F}\boldsymbol{S}\boldsymbol{F}^T\ , \qquad \text{or} \qquad \tau^{ab} = F^a{}_A S^{AB} F^b{}_B\ . \tag{18}$$

2.3. Maxwell's Laws for Electrostatics

The aim of this section is to set Maxwell's equations for the case of electro-quasistatics in dielectric media. On top constitutive equations will be introduced using an approach

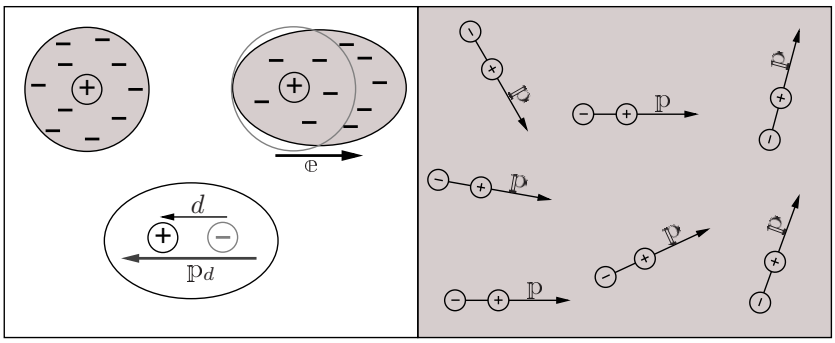

Figure 7: Microscopic (left image) and macroscopic(right image) interpretation of polarization vector in a dielectric media. In the presence of an electric field the charge cloud is in the atomic level is distorted, and this can be reduced to a simple dipole model. A dipole is characterized by its dipole moment $\mathbb{p}_d$.

similar to continuum mechanics. Furthermore, geometrical transformation of these physical laws will be addressed in order to have them in both natural Eulerian $\mathcal{S}$ and also Lagrangian $\mathcal{B}$ configurations.

2.3.1. Gauss's Law. *Gauss' law* describes the relationship between an electric field and its generating electric charges. In the field line description, electric field lines begin only at positive electric charges and end only at negative electric charges. 'Counting' the number of field lines in a closed surface, therefore, yields the total charge enclosed by that surface. More technically, *Gauss' law states that the electric flux through any hypothetical closed "Gaussian surface" is identical to the total electric charge within the surface.*

$$\oint_{\partial\mathcal{S}} \mathbb{e} \cdot d\boldsymbol{s} = \frac{q_{tot}}{\epsilon_0} \tag{19}$$

In equation (19), $\mathbb{e}$ stands for the electric field in Eulerian configuration and q_{tot} is the total electric charge in closed surface $\partial\mathcal{S}$.

In the classical approach to the dielectric material model, a material is made up of atoms. Each atom consists of a cloud of negative charge (Electrons) bound to and surrounding a positive point charge at its center. In the presence of an electric field the charge cloud is distorted, Figure (20), and this can be reduced to a simple dipole model. A dipole is characterized by its dipole moment, a vector quantity shown in Figure (20) as $\mathbb{p}_d$. In general, macroscopic model for the effect of electric field on matter can be motivated by the microscopic model described here. To characterize electric field matter interaction we define polarization $\mathbb{p}_d$. Polarization can also be result of *Dipolar polarization* (rotation and reorientation of randomely aligned permanent polarized molecules) and *Ionic polarization*(relative displacements between positive and negative ions). However all of them will result in a macroscopically polarization vector field that is defined in terms of $\mathbb{p}_d$.

$$\mathbb{p} = \frac{1}{\Delta v}\sum \mathbb{p}_d \qquad , \qquad \mathbb{p}_d = q \cdot \mathbf{d} \tag{20}$$

Here, q is the atomic charge, $\mathbf{d}$ is distance between charges in microscopic level and $\mathbb{p}$ is macroscopic polarization in the current configuration. In a dielectric media, gradient of polarization cause a resultant negative charge. This fact is formally shown in Equation (21) and motivated in Figure (8).

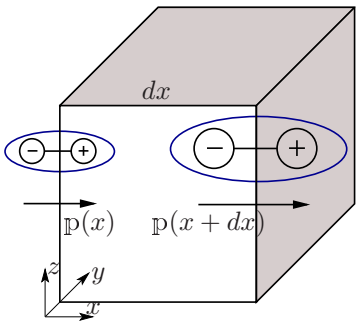

Figure 8: Polarization gradient result in a volume charge density. This can be seen from the difference of charges in the opposite sides of volume element shown in the picture.

$$\mathrm{div}[\mathbb{p}(\boldsymbol{x})] = -\rho^b \qquad , \qquad \sigma_b = \mathbb{p}\cdot\mathbf{n} \tag{21}$$

In Equation (21), σ^b stands for bound charge surface density and ρ^b is called volume density of polarization charge or bound charge density.
To apply Gauss's law, Equation (19), in a dielectric media one must consider both free charge density and polarization charge density. If we define two parts of q_{tot} as q_b and q_f, the following relation will be obtained.

$$\oint_{\partial\mathcal{S}} \mathbb{e}\cdot d\boldsymbol{s} = \frac{q_f + q_b}{\epsilon_0} \tag{22}$$

As it can be seen in Equation (22) total charge that enters Maxwell's equation is given by $\rho^t = \rho^f + \rho^b$. Using Divergence theorem in parallel with Equation (21) and localization theorem Equation (22) can be expressed in differential form.

$$\mathrm{div}[\epsilon_0\mathbb{e} + \mathbb{p}] = \rho^f \tag{23}$$

In practice it is inconvenient to take explicit account for polarization, Therefore, the electric displacement field $\mathbb{d}$ is defined and Equation (23) is rewritten in essential form of Gauss theorem in dielectrics. Furthuremore, we can obtain boundary condition of this equation using boundary condition of Equation (21).

$$\begin{gathered} \mathbb{d} = \epsilon_0\mathbb{e} + \mathbb{p} \\ \mathrm{div}[\mathbb{d}] = \rho^f \qquad , \qquad \sigma^f = \mathbb{d}\cdot\mathbf{n} \end{gathered} \tag{24}$$

Electric displacement $\mathbb{d}$, also known as electric flux density, is the charge per unit area that would be displaced across a layer of conductor placed across an electric field. This quantity describes also the density of electric flux passing through a Gaussian surface ∂S in an electric field. In order to specify the relation betweeen displacement field and electric field we will need costitutive equation. This equation specify the response of bound charge and current to the applied fields and is called constitutive relation. Linear relation between true displacement and electric fiels is a typical experimentally verified constitutive law for Dielectric Elastomers(Plante & Dubowsky [19]). Here ϵ is dielectric permitivity of the dielectric media.

$$\mathbb{d} = \epsilon\mathbb{e} \tag{25}$$

Box 1: Boundary-Value-Problem of Electrostatics.

1. Kinematics

$$\mathbb{e} = -\nabla_{\boldsymbol{x}}\phi^e(\boldsymbol{x}) \qquad (\mathrm{curl}[\mathbb{e}] = 0). \tag{26a}$$

2. Equilibrium equations

$$\mathrm{div}[\mathbb{d}(\boldsymbol{x})] = \rho^e(\boldsymbol{x}). \tag{26b}$$

3. Constitutive relation

$$\mathbb{d}(\boldsymbol{x}) = \hat{\mathbb{d}}(\mathbb{e}) = \epsilon\mathbb{e}. \tag{26c}$$

4. Boundary conditions

$$\begin{aligned} \mathbb{d}(\boldsymbol{x})\cdot\boldsymbol{n} &= -\sigma^e(\boldsymbol{x},\boldsymbol{n}), \quad \text{on } \partial\mathcal{S}_{\mathbb{d}} \quad \text{on} \\ \phi^e(\boldsymbol{x}) &= \bar{\phi}^e(\boldsymbol{x}), \qquad \text{on } \partial\mathcal{S}_{\phi}. \quad \text{on} \end{aligned} \tag{26d}$$

2.3.2. Faraday's law of induction. In Electromagnetic physics, a quantitative relationship between a *changing magnetic field* and the electric field created by the change, developed on the basis of experimental observations made in 1831 by the English scientist *Michael Faraday*. Years later the Scottish physicist *James Clerk Maxwell* proposed that the fundamental effect of changing magnetic flux was the production of an electric field, not only in a conductor but also in space even in the absence of electric charges. In other words: *A changing magnetic field creates an electric field*. This can be shown in the mathematical language like:

$$\mathrm{curl}[\mathbb{e}] = -\frac{\partial\mathbb{b}}{\partial t} \tag{27}$$

Transient simulations under the *electro-quasistatic (EQS)* assumption are typically performed for the electrodynamic analysis of technical applications which arise from high-voltage technology or microelectronics if they are operated at low frequencies. The EQS assumption is applicable if electromagnetic wave propagation effects can be disregarded and if the electric energy density of the problem is considerably larger than the magnetic energy density(see e.g. Steinmetz et al. [24]). This is exactly coinciding with the desired simulation condition of this work. Capacitive as well as resistive material behavior can be taken into account under EQS assumption.
Under the EQS assumption, derivative of magnetic field is approaching zero and a scalar electric potential function ϕ^e for the irrotational electric field strength can be introduced. This potential function $\phi^e(\boldsymbol{x})$ is called *electric potential* of the point $\boldsymbol{x}$ and is defined as the elctromotive force i.e. $\mathbb{e}\cdot d\boldsymbol{l}$, from $\boldsymbol{x}$ to an arbitrary reference point $\boldsymbol{x}_0$.

$$\mathrm{curl}[\mathbb{e}] = 0 \qquad \Longrightarrow \qquad \mathbb{e} = -\nabla_{\boldsymbol{x}}\phi^e(\boldsymbol{x}) \quad , \quad \phi^e(\boldsymbol{x}) = -\int_{\boldsymbol{x}_0}^{\boldsymbol{x}} \mathbb{e}\cdot d\boldsymbol{l} \tag{28}$$

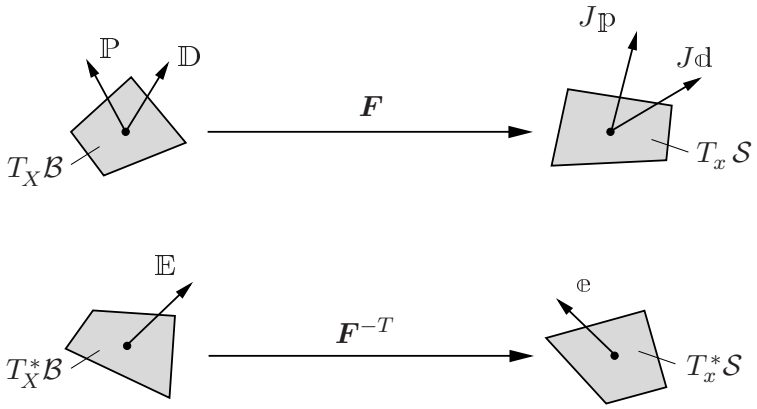

Figure 9: Commutative diagram illustrating the geometric mapping relations between material and spatial electric field variables.

2.3.3. Boundary-Value Problem of Electrostatistics. Using *Gauss's* and *Faraday's* law one can summerize the boundary-value-problem for the electrostatic case in a given region $\mathcal{S} \subset \mathbb{R}^3$ occupied by a dielectric material and surrounded by free space as in Box(1). Here the boundary $\partial\mathcal{S}$ has been decomposed in a portion $\partial\mathcal{S}_{\mathbb{d}}$, where the free surface charges are placed, and a portion $\partial\mathcal{S}_{\phi^e}$, where the electric potential can be assigned.

$$\partial\mathcal{S} = \partial\mathcal{S}_{\mathbb{d}} \cup \partial\mathcal{S}_{\phi^e} \quad \text{with} \quad \partial\mathcal{S}_{\mathbb{d}} \cap \partial\mathcal{S}_{\phi^e} \in \emptyset \tag{29}$$

2.3.4. Geometrical Transformations of Electrical Objects. By using the definition of electric potential and transformation of line elements in Equation (28), we can transform the integration on the actual configuration in an integration on the reference configuration and define the Lagrangian electric field $\mathbb{E}$ as follows.

$$\phi^e(\boldsymbol{x}) = -\int_{\boldsymbol{x}_0}^{\boldsymbol{x}} \mathbb{e} \cdot d\boldsymbol{l} = -\int_{\boldsymbol{X}_0}^{\boldsymbol{X}} \boldsymbol{F}^{-T}\mathbb{e} \cdot d\boldsymbol{L} = -\int_{\boldsymbol{X}_0}^{\boldsymbol{X}} \mathbb{E} \cdot d\boldsymbol{L} \tag{30}$$

yielding the transormation

$$\mathbb{e} = \boldsymbol{F}^{-T}\mathbb{E} \tag{31}$$

As $\boldsymbol{F}^{-T}$ being the normal map, we identify $\mathbb{e}$ as a geometric object of the Eulerian cotangent space $T_x^*\mathcal{S}$ and $\mathbb{E}$ as an object of the Lagrangian cotangent space $T_X^*\mathcal{B}$ (cf. Figure 9).

Within a silmilar approach, using the integral form of equation (24), and surface element transformation one can define Lagrangian electric displacement $\mathbb{D}$ and polarization $\mathbb{P}$ fields.

$$q^e[\partial\mathcal{S}] = \int_{\partial\mathcal{S}} \mathbb{d} \cdot d\boldsymbol{s} = \int_{\partial\mathcal{B}} \mathbb{d} \cdot J\boldsymbol{F}^{-T} d\boldsymbol{S} = \int_{\partial\mathcal{B}} J\boldsymbol{F}^{-1}\mathbb{d} \cdot d\boldsymbol{S} = \int_{\partial\mathcal{B}} \mathbb{D} \cdot d\boldsymbol{S} \tag{32}$$

Same relations hold for polarization field due to the same characteristics of these two variables. Thus the transformation of elctric displacement and polarization fields reads as follows.

$$\mathbb{d} = J^{-1}\boldsymbol{F}\mathbb{D} \quad , \quad \mathbb{p} = J^{-1}\boldsymbol{F}\mathbb{P} \tag{33}$$

This transformation is a typical Piola-transformation and allow us to identify $J\mathbb{d}$ and $J\mathbb{p}$ as geometric objects of Eulerian tangent space $T_x\mathcal{S}$. In the same way $\mathbb{D}$ and $\mathbb{P}$ are objects of Lagrangian tangent space $T_X\mathcal{B}$. It is worth pointing out that due to the different geometrical natures of the electric field, the electric displacement, and the polarization, we need to modify Equation (24) as follows.

$$\mathbb{p} = \mathbb{d} - \epsilon_0 \boldsymbol{g}^{-1}\mathbb{e} \tag{34}$$

2.4. Extended Balance Laws of Continuum Thermodynamics

In this section the balance principles of continuum thermomechanics are briefly reviewed and the main focus is placed on their extension to the continuum mechanics of polarizable matter. This step requires the addition of terms in the thermomechanical balance laws, as well as the introduction of Maxwell's equations. Extensive discussions of the *electrodynamics of continua* have been presented by Pao & Hutter [17], Hutter & van de Ven [10], Maugin [14], Eringen and Maugin [5].

For any *admissible thermo-electro-mechanical process* the following global balance laws must hold for every part $\mathcal{P}_t \subset \mathcal{S}$ of the material body, along with the Electrostatic equations introduced in the section 2.3. These balance equations contain, in addition to the classical contributions, the *electrical body force field* $\rho\boldsymbol{\gamma}^e(\boldsymbol{x},t)$, the *electrical body couple field* $\rho\boldsymbol{m}^e(\boldsymbol{x},t)$ and the *electrical energy source field* $\rho r^e(\boldsymbol{x},t)$, which are due to the *field-matter-interactions* of the deforming polarizable body and the electric field.[2]

In the following equations $\mathfrak{M}$ denotes the *mass*, $\mathfrak{L}$ the *linear momentum*, $\mathfrak{F}$ the *resultant electromechanical force*, $\mathcal{A}_0$ the *angular momentum* and $\mathfrak{M}_0$ the *resultant electromechanical moment* about the origin, $\mathfrak{K}$ the *kinetic energy*, $\mathfrak{E}$ the *internal energy*, $\mathfrak{P}$ the *power due to external electromechanical forces*, $\mathfrak{Q}$ the sum of *thermal and electromechanical power*, Γ the *total rate of entropy production*, $\mathfrak{H}$ the *entropy* and finally $\mathfrak{S}$ the *entropy power* of the considered part $\mathcal{P}_t$.

Furtheremore, in the bellow formulation, ρ is the *mass density per unit volume*, ρ_0 is the *mass density per unit volume of reference configuration*, $\boldsymbol{\gamma}$ is the *total body force due to electric fields and external actions*, $\boldsymbol{m}$ is *body couple in actual configuration*, e is *internal energy per unit mass*, $\boldsymbol{q}$ is the *heat flux* and r is *total energy supply due to electromagnetic fields and to heat per unit mass*. Also, $\hat{\boldsymbol{m}}^e$ is dual second order tensors to the electric body couple, i.e. for a generic vector $\boldsymbol{x}$, we can write; $\hat{\boldsymbol{m}}^e\boldsymbol{x} = \boldsymbol{m}^e \times \boldsymbol{x}$. It is assumed that body force, body couple and energy supply can be decomposed into seperate electric and nonelectric parts. The electric part will be expressed in terms of electrical quantities, and indicated with the superscript "e", the other is supposed to be externally applied and known from the outset and contradistinguished with a bar. Hence:

$$\rho\boldsymbol{\gamma} = \rho\boldsymbol{\gamma}^e + \rho\bar{\boldsymbol{\gamma}} \quad , \quad \rho\boldsymbol{m} = \rho\boldsymbol{m}^e \quad , \quad \rho r = \rho r^e + \rho\bar{r} \tag{35}$$

Furthuremore, relation between material and current configuration parameters are as follows:

$$\boldsymbol{P} = J\boldsymbol{\sigma}\boldsymbol{F}^{-T} \quad , \quad \boldsymbol{Q} = J\boldsymbol{F}^{-1}\boldsymbol{q}$$

[2]The specific form of electromagnetic source terms depends on the underlying model for field matter interactions, such as the *dipole–dipole*, or the *dipole–current loop* models discussed for example in [10], [17].

$$\boldsymbol{\Gamma}(\boldsymbol{X},t)=\boldsymbol{\gamma}(\boldsymbol{x},t)\circ\varphi_t(\boldsymbol{x},t) \qquad , \qquad \boldsymbol{M}(\boldsymbol{X},t)=\boldsymbol{m}(\boldsymbol{x},t)\circ\varphi_t(\boldsymbol{x},t) \tag{36}$$

With these definitions at hand, one can express the *global balance laws of continuum thermodynamics for polarizable media in the spatial setting* in the following form

Balance of mass

$$\frac{d}{dt}\mathfrak{M}=0\ , \quad \frac{d}{dt}\int\limits_{\mathcal{P}_t}\rho\,dv=0\ . \tag{37a}$$

Balance of linear momentum

$$\frac{d}{dt}\boldsymbol{\mathcal{L}}=\boldsymbol{\mathcal{F}}\ , \quad \frac{d}{dt}\int\limits_{\mathcal{P}_t}\rho\boldsymbol{v}\,dv=\int\limits_{\mathcal{P}_t}\left[\rho\bar{\boldsymbol{\gamma}}+\rho\boldsymbol{\gamma}^e\right]\,dv+\int\limits_{\partial\mathcal{P}_t}\boldsymbol{t}\,da\ . \tag{37b}$$

Balance of angular momentum

$$\frac{d}{dt}\boldsymbol{\mathcal{A}}_0=\boldsymbol{\mathfrak{M}}_0\ , \quad \frac{d}{dt}\int\limits_{\mathcal{P}_t}\boldsymbol{x}\times\rho\boldsymbol{v}\,dv=\int\limits_{\mathcal{P}_t}\left[\boldsymbol{x}\times(\rho\bar{\boldsymbol{\gamma}}+\rho\boldsymbol{\gamma}^e)+\rho\boldsymbol{m}^e\right]\,dv+\int\limits_{\partial\mathcal{P}_t}\boldsymbol{x}\times\boldsymbol{t}\,da\ . \tag{37c}$$

Balance of energy (first law of thermodynamics)

$$\frac{d}{dt}\left(\mathfrak{K}+\mathfrak{E}\right)=\mathfrak{P}+\mathfrak{Q}\ , \tag{37d}$$

$$\frac{d}{dt}\int\limits_{\mathcal{P}_t}\left[\,\tfrac{1}{2}\,\rho\boldsymbol{v}\cdot\boldsymbol{g}\boldsymbol{v}+\rho e\right]\,dv=\int\limits_{\mathcal{P}_t}\left[(\rho\bar{\boldsymbol{\gamma}}+\rho\boldsymbol{\gamma}^e)\cdot\boldsymbol{g}\boldsymbol{v}\right]\,dv+\int\limits_{\partial\mathcal{P}_t}\boldsymbol{t}\cdot\boldsymbol{g}\boldsymbol{v}\,da + \int\limits_{\mathcal{P}_t}\rho\bar{r}\,dv-\int\limits_{\partial\mathcal{P}_t}\boldsymbol{q}\cdot\boldsymbol{n}\,da+\int\limits_{\mathcal{P}_t}\rho r^e\,dv\ .$$

Entropy inequality (second law of thermodynamics)

$$\Gamma:=\frac{d}{dt}\mathfrak{H}-\mathfrak{S}\geq 0\ , \quad \int\limits_{\mathcal{P}_t}\rho\gamma\,dv:=\frac{d}{dt}\int\limits_{\mathcal{P}_t}\rho\eta\,dv-\left(\int\limits_{\mathcal{P}_t}\frac{\rho\bar{r}}{\theta}\,dv-\int\limits_{\partial\mathcal{P}_t}\frac{\boldsymbol{q}\cdot\boldsymbol{n}}{\theta}\,da\right)\geq 0\ . \tag{37e}$$

By using standard divergence, transport and localization theorems as well as the geometric mappings introduced above, the *local balance laws of continuum thermodynamics for polarizable media in the spatial* and *material settings* are derived as

Balance of mass

$$\dot{\rho}+\rho\,\mathrm{div}\,\boldsymbol{v}=0\ , \qquad J\rho(\boldsymbol{\varphi}_t(\boldsymbol{X}),t)=\rho_0(\boldsymbol{X})\ . \tag{38a}$$

Balance of linear momentum

$$\rho\dot{\boldsymbol{v}}=\mathrm{div}\,\boldsymbol{\sigma}+\rho\bar{\boldsymbol{\gamma}}+\rho\boldsymbol{\gamma}^e\ , \qquad \rho_0\dot{\boldsymbol{V}}=\mathrm{Div}\,\boldsymbol{P}+\rho_0\bar{\boldsymbol{\Gamma}}+\rho_0\boldsymbol{\Gamma}^e\ . \tag{38b}$$

Balance of angular momentum

$$\operatorname{skew}\boldsymbol{\sigma} = \rho\hat{\boldsymbol{m}}^e \ , \qquad \operatorname{skew}\left(\boldsymbol{P}\boldsymbol{F}^T\right) = \rho_0\hat{\boldsymbol{M}}^e \ . \tag{38c}$$

Balance of energy (first law of thermodynamics)

$$\rho\dot{e} = \boldsymbol{\sigma} : \boldsymbol{g}\boldsymbol{l} + \rho\bar{r} - \operatorname{div}\boldsymbol{q} + \rho r^e \ , \qquad \rho_0\dot{e} = \boldsymbol{g}\boldsymbol{P} : \dot{\boldsymbol{F}} + \rho_0\bar{R} - \operatorname{Div}\boldsymbol{Q} + \rho_0 R^e \ . \tag{38d}$$

Entropy inequality (second law of thermodynamics)

$$\rho\gamma = \rho\dot{\eta} - \rho\,\frac{\bar{r}}{\theta} + \frac{1}{\theta}\operatorname{div}\boldsymbol{q} - \frac{1}{\theta^2}\,\boldsymbol{q}\cdot\operatorname{grad}\theta \geq 0 \ , \tag{38e}$$

$$\rho_0\gamma = \rho_0\dot{\eta} - \rho_0\,\frac{\bar{R}}{\theta} + \frac{1}{\theta}\operatorname{Div}\boldsymbol{Q} - \frac{1}{\theta^2}\,\boldsymbol{Q}\cdot\operatorname{Grad}\theta \geq 0 \ . \tag{38f}$$

The balance laws for polarizable continua listed above are general. As mentioned, however, they require the specification of the electromotive force and couple terms as well as the electrical energy source term. These terms must be justified based on a particular field-matter-interactions theory. There are several approaches regarding the specification of these terms. For a broader discussion of this deep subject the reader is referred to [10]. The model that will be adopted here, mainly because of its intuitiveness, mathematical simplicity and the resulting "symmetry" of electric and magnetic effects, is the *two-dipole model* in the so-called *Chu Formulation*, as discussed in detail by Pao & Hutter [16, 17].

Restricting ourselves to purely electric effects for the present purpose, the field-matter-interaction source terms of the two-dipole model are given by [10]

$$\rho\boldsymbol{\gamma}^e = [\nabla_{\boldsymbol{x}}\mathbb{e}(\boldsymbol{x})]\mathbb{p} + \rho^f\mathbb{e} \quad , \quad \rho\hat{\boldsymbol{m}}^e = \operatorname{skew}[\mathbb{p}\times\mathbb{e}] \quad , \quad \rho r^e = \rho\mathbb{e}\cdot\frac{d}{dt}(\frac{\mathbb{p}}{\rho}) \ . \tag{39}$$

2.4.1. Modified Balance Equations Using Maxwell's Stress Tensor. The Maxwell stress tensor σ^M is a second rank tensor used in classical electromagnetism to represent the interaction between electric/magnetic forces and mechanical momentum. It is defined such that:

$$\operatorname{div}[\boldsymbol{\sigma}^M] = \rho\boldsymbol{\gamma}^e \qquad , \qquad \operatorname{skew}[\boldsymbol{\sigma}^M] = \rho\hat{\boldsymbol{m}}^e \tag{40}$$

With the introduction of Maxwell's stress tensor, the conservation of linear momentum can be rewritten as:

$$\rho\dot{\boldsymbol{v}} = \operatorname{div}[\boldsymbol{\sigma}] + \rho\bar{\boldsymbol{\gamma}} + \rho\boldsymbol{\gamma}^e \qquad \Rightarrow \qquad \rho\dot{\boldsymbol{v}} = \operatorname{div}[\boldsymbol{\sigma}] + \rho\bar{\boldsymbol{\gamma}} + \operatorname{div}[\boldsymbol{\sigma}^M] \tag{41}$$

Defining the total stress as $\boldsymbol{\sigma}^{tot} = \boldsymbol{\sigma} + \boldsymbol{\sigma}^M$ we can rewrite conservation of linear momentum as:

$$\rho\dot{\boldsymbol{v}} = \operatorname{div}[\boldsymbol{\sigma}^{tot}] + \rho\bar{\boldsymbol{\gamma}} \tag{42}$$

Reminding that $\bar{\boldsymbol{\gamma}}$ is just the mechanical internal forces. The total stress tensor has the advantage of being symmetric, i.e. the balance of angular momentum takes the form:

$$\operatorname{skew}[\boldsymbol{\sigma}^{tot}] = 0 \tag{43}$$

For the two-dipole model in the Chu formulation considered here the following form of the Maxwell stress tensor is formulated

$$\boldsymbol{\sigma}^M = \epsilon_0 \mathbb{e} \otimes \mathbb{e} + \mathbb{e} \otimes \mathbb{p} - \frac{1}{2}\epsilon_0 |\mathbb{e}|^2 \mathbf{1} = \mathbb{e} \otimes \mathbb{d} - \frac{1}{2}\epsilon_0 |\mathbb{e}|^2 \mathbf{1} \tag{44}$$

It can be shown that this definition is fulfills properties discussed above (see e.g. Rosato [21]. With this new definition of stress, i.e. $\boldsymbol{\sigma}^{tot} = \boldsymbol{\sigma} + \mathbb{e} \otimes \mathbb{d} - \frac{1}{2}\epsilon_0 |\mathbb{e}|^2 \mathbf{1}$, the total stress should be considered as total Cauchy stress tensor. Modified balance equations (42) and (43) are written in the deformed configuration. In an analogous way, we can define a total first Piola stress.

$$\boldsymbol{P}^{tot} = \boldsymbol{P} + \boldsymbol{P}^M \qquad with \qquad \boldsymbol{P}^M = \boldsymbol{F}^{-T}\boldsymbol{E} \otimes \boldsymbol{D} - \frac{1}{2} J \epsilon_0 (\boldsymbol{C}^{-1} : \mathbb{E} \otimes \mathbb{E}) \boldsymbol{F}^{-T} := J \boldsymbol{\sigma}^M \boldsymbol{F}^{-T} \tag{45}$$

Summerizing, modified balance equations considering total stress instead of mechanical stress in deformesd and undeformed configuration reads:

$$\begin{aligned} \rho_0 \dot{\boldsymbol{V}} &= \operatorname{div}[\boldsymbol{P}^{tot}] + \rho_0 \bar{\boldsymbol{\Gamma}} \quad \text{in} \quad \mathcal{B} \\ \operatorname{skew}[\boldsymbol{P}^{tot} \boldsymbol{F}^T] &= 0 \qquad\quad \text{in} \quad \mathcal{B} \end{aligned} \tag{46}$$

2.5. Fully-Coupled Boundary Value Problems

Putting together both mechanical and electrical balance laws we shall obtain a system of *fully-coupled boundary value problem for elctromechanics*. We consider in this work a formulation of the local constitutive material response based on a set of independent variables which have a geometric character. For simple future recalling we will use a description in terms of generalized vectors $\mathfrak{S}$ and generalized covectors $\mathfrak{F}$ that is used by Rosato [21]. Generalized vectors are the those contravariant objects having basis in the tangent spaces. In the framework discussed here stress and electric displacement are variable that we can apply Cauchy-type theorem on both of them and they represent the generalized vectors here. The dual quantities which can be then considered as the generalized covectors are deformations and electric field.

$$\mathfrak{S}' := [\boldsymbol{g}\boldsymbol{P}^{tot}, -\mathbb{D}] \quad , \quad \mathfrak{F}' := [\boldsymbol{F}, \mathbb{E}] \tag{47}$$

Regarding to the boundary conditions, in an electromechanical formulation, the body may contain a discontinuity surface Γ_d over which the electro-mechanical field variables can suffer jumps. Across a surface of discontinuity within the boundary or across the boundary $\partial\mathcal{S}$, the fields $\mathbb{e}$ and $\mathbb{d}$ have to satisfy certain continuity conditions. Here, we do not consider internal surfaces of discontinuity and therefore the continuity conditions refer only to $\partial\mathcal{S}$. Then the continuity conditions satisfied by the electric field and electric displacement are

$$[\![\mathbb{e}]\!] \times \boldsymbol{n} = \mathbf{0} \quad \text{and} \quad [\![\mathbb{d}]\!] \cdot \boldsymbol{n} = \sigma^f \quad \text{on} \quad \partial\mathcal{S} \tag{48}$$

with σ^f surface charge density and $[\![\boldsymbol{a}]\!] := \boldsymbol{a}^+ - \boldsymbol{a}^-$ denotes the jump of a quasntity $\boldsymbol{a}$ across $\partial\mathcal{S}$. The sides of the surface is identified by the direction of its outward normal. To complete the formulation of well-posed boundary value problems in finite electrome-

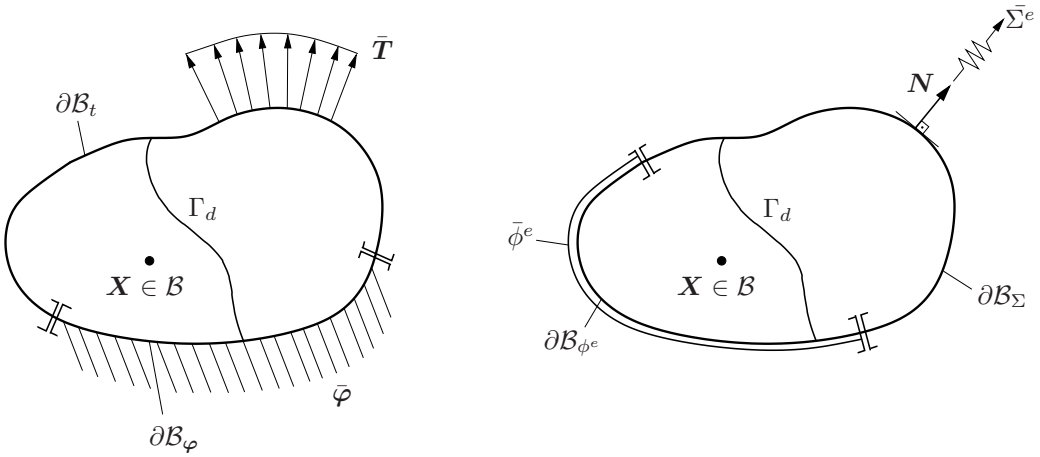

Figure 10: Visualization of the mechanical and electrical boundary conditions on the surface segments $\partial\mathcal{B} = \partial\mathcal{B}_{\boldsymbol{\varphi}} \cup \partial\mathcal{B}_T$ or $\partial\mathcal{B} = \partial\mathcal{B}_{\phi^e} \cup \partial\mathcal{B}_\Sigma$ of the body in the reference configuration.

chanics, appropriate boundary conditions for balance equations must be specified. One considers the material body $\mathcal{B}$ depicted in Figure (10), whose surface is considered to be subdivided into the non-overlapping segments $\partial\mathcal{B}_{\boldsymbol{\varphi}}$ and $\partial\mathcal{B}_T$, such that $\partial\mathcal{B} = \partial\mathcal{B}_{\boldsymbol{\varphi}} \cup \partial\mathcal{B}_T$ and $\partial\mathcal{B}_{\boldsymbol{\varphi}} \cap \partial\mathcal{B}_T \in \emptyset$ from the mechanical viewpoint, and into the segments $\partial\mathcal{B}_{\phi^e}$ and $\partial\mathcal{B}_\Sigma$, with $\partial\mathcal{B} = \partial\mathcal{B}_{\phi^e} \cup \partial\mathcal{B}_\Sigma$ and $\partial\mathcal{B}_{\phi^e} \cap \partial\mathcal{B}_\Sigma \in \emptyset$, in the electric case. There exists of course no general restrictions on how the mechanical and electrical surface segments might overlap.

The appropriate *Dirichlet and Neumann-type* mechanical and electrical *boundary conditions* to be applied to the respective boundary segments are given by

$$\begin{aligned} &\boldsymbol{\varphi} = \bar{\boldsymbol{\varphi}} \ , \quad \text{on } \partial\mathcal{B}_{\boldsymbol{\varphi}} \ , \qquad \boldsymbol{P}^{tot}\boldsymbol{N} = \bar{\boldsymbol{T}} \ , \qquad\qquad \text{on } \partial\mathcal{B}_T \ , \\ &\phi^e = \bar{\phi^e} \ , \quad \text{on } \mathcal{B}_{\phi^e} \ , \qquad [\![\mathbb{D}]\!] \cdot \boldsymbol{N} = \bar{\Sigma^e} \quad \text{and} \quad [\![\mathbb{E}]\!] \times \boldsymbol{N} = \boldsymbol{0} \ , \quad \text{on } \partial\mathcal{B}_\Sigma \ . \end{aligned} \tag{49}$$

We have thus completed the derivation of the geometrically and physically-nonlinear problem of (static) electromechanics at finite strains.

The complete set of the associated governing equations is summarized using generalize dvectors and covectors bellow.

Kinematics: introduce the generalized deformation map $\mathfrak{U} := [\boldsymbol{\varphi}(\boldsymbol{X}, t), -\phi^e(\boldsymbol{X}, t)]^T$, the generalized covector $\mathfrak{F} := [\boldsymbol{F}, \mathbb{E}]^T$ and the generalized gradient operator $\mathscr{G}$

$$\mathfrak{F} := \mathscr{G}[\mathfrak{U}] \qquad \text{or} \qquad [\boldsymbol{F}, \mathbb{E}]^T := [\nabla_{\boldsymbol{X}}\boldsymbol{\varphi}, -\nabla_{\boldsymbol{X}}\phi^e]^T \tag{50a}$$

Equilibrium Equations: introduce the generalized vector $\mathfrak{S} := [\boldsymbol{g}\boldsymbol{P}, -\mathbb{D}]^T$, the generalized divergence operator $\mathscr{D}_v$ and the generalized body forces $\bar{\mathfrak{B}} := [\rho_0\bar{\boldsymbol{\Gamma}}, \rho^f]^T$

$$\mathscr{D}_v[\mathfrak{S}] + \bar{\mathfrak{B}} = \boldsymbol{0} \qquad \text{or} \qquad \mathrm{Div}[\boldsymbol{P}, -\mathbb{D}]^T + [\rho_0\bar{\boldsymbol{\Gamma}}, \rho^f]^T = [\boldsymbol{0}, 0]^T \tag{50b}$$

Boundary Conditions: Assemble the Dirichlet boundaries $\partial\mathcal{B}_{\mathfrak{U}} := \{\partial\mathcal{B}_{\boldsymbol{\varphi}}, \partial\mathcal{B}_\phi\}$, the Neumann boundaries $\partial\mathcal{B}_{\mathfrak{T}} := \{\partial\mathcal{B}_{\boldsymbol{T}}, \partial\mathcal{B}_\Sigma\}$ and the generalized normal vector $\mathfrak{N} := [\boldsymbol{N}, \boldsymbol{N}]^T$

$$\mathfrak{U} = \bar{\mathfrak{U}} \quad \text{on} \quad \partial\mathcal{B}_{\mathfrak{U}} \quad \text{and} \quad \mathfrak{S} \cdot \mathfrak{N} = \bar{\mathfrak{T}} \quad \text{on} \quad \partial\mathcal{B}_{\mathfrak{T}} \tag{50c}$$

3. Finite Electro-Elasticity

The ultimate goal of this chapter is to develop appropriate material model for Dielectric Elastomers. The solution of the balance equations in combination with the constitutive equations gives us the electro-mechanical fields within the region under consideration.

3.1. Thermodynamically-Consistent Constitutive Theory

A continuum constitutive theory is considered to be *thermodynamically-consistent* if it satisfies the fundamental balance equations of continuum mechanics and the laws of thermodynamics derived in the previous section at each material point (see also Coleman & Noll [4]). It is assumed that all thermodynamic properties of the material can be characterized by a (scalar-valued) *thermodynamic potential*, such as the *specific internal energy* previously introduced in the energy balance (37d). Following the *Coleman and Noll method* it is possible to derive general constitutive relations for the dependent field variables in the form of gradients to the thermodynamic potential, such that thermodynamic consistency is guaranteed a priori.

3.2. Enthropy Inequality

It is a fact of experience that real physical processes are irreversible. This means that processes cannot, in general, be traversed back in time. This fact is called the second law of thermodynamics and its mathematical realization is the entropy production inequality. It is based on the assumption that there exists a quantity η, called the entropy, which satisfy the following balance:

$$\frac{d}{dt}\int\limits_{\mathcal{P}_\mathcal{S}} \rho\eta dv = \int\limits_{\mathcal{P}_\mathcal{S}} \rho\gamma dv + \left(\int\limits_{\partial\mathcal{P}_\mathcal{S}} \rho\frac{\bar{r}}{\theta} dv - \int\limits_{\partial\mathcal{P}_\mathcal{S}} \frac{\boldsymbol{q}\cdot\boldsymbol{n}}{\theta} da \right) \tag{51}$$

Here γ is the rate of enthropy production, η the total entropy of the system contained in $\partial\mathcal{S}$, $\bar{r}/\theta$ the enthropy supplied with the heat and $(\boldsymbol{q}\cdot\boldsymbol{n})/\theta$ is the enthropy flux with the heat flux $\boldsymbol{q}\cdot\boldsymbol{n}$ over the absolute temperature θ. The second law of thermodynamics states that the enthropy production γ is always positive because of occurrence of irreversible processes. Thus for sufficiently smooth fields (51) implies the Clausius-Duhem-Inequality.

$$\rho\gamma = \rho\dot{\eta} - \rho\frac{\bar{r}}{\theta} + \frac{1}{\theta}\mathrm{div}[\boldsymbol{q}] - \frac{1}{\theta^2}\boldsymbol{q}\cdot\nabla_{\boldsymbol{x}}\theta \geq 0 \tag{52}$$

The volume specific spatial dissipation is defined as the product of the rate of entropy production in (52) with the absolute temperature θ, i.e. $J\mathscr{D} = \rho\gamma\theta \geq 0$, in which $\mathscr{D}$ is defined as dissipation per unit reference volume. Owing to the nature of terms in (52), it is common practice to additively split the dissipation into the local $\mathscr{D}_{loc}$ and $\mathscr{D}_{con}$ parts, $J\mathscr{D} = J\mathscr{D}_{loc} + J\mathscr{D}_{loc}$. We then require a stricter condition than (52) by demanding the positiveness of both terms $\mathscr{D}_{loc}$ and $\mathscr{D}_{con}$ separately. To this end, we introduce the Clausius-Planck-Inequality (CPI in the following),

$$J\mathscr{D}_{loc} = \rho\dot{\eta}\theta - (\rho\bar{r} - \mathrm{div}[\boldsymbol{q}]) \tag{53}$$

and the Fourier inequality (FI).

$$J\mathscr{D}_{con} = -\frac{1}{\theta}\boldsymbol{q}\cdot\nabla_{\boldsymbol{x}}\theta \geq 0 \tag{54}$$

Incorporating the spatial energy balance equation in the CPI we get a formulation of this inequality in terms of the internal energy in actual configuration.

$$J\mathscr{D}_{loc} = \boldsymbol{\sigma} : \boldsymbol{gl} + \rho\dot{\eta}\theta + \rho r^e - \rho\dot{e} \tag{55}$$

The FI and CPI could be also written in the reference configuration as follows.

$$\mathscr{D}_{con} = -\frac{1}{\theta}\boldsymbol{Q}\cdot\nabla_{\boldsymbol{X}}\theta \geq 0 \tag{56}$$

$$\mathscr{D}_{loc} = \boldsymbol{gP} : \dot{\boldsymbol{F}} + \rho_0\dot{\eta}\theta + \rho_0 R^e - \rho_0\dot{e} \geq 0 \tag{57}$$

By choosing the two-dipole model for the description of the electric body force, body couple and energy supply, it follows that

$$\mathscr{D}_{loc} = [\boldsymbol{gP} + \boldsymbol{F}^{-T}(\mathbb{E}\otimes\mathbb{P})] : \dot{\boldsymbol{F}} + \mathbb{E}\cdot\dot{\mathbb{P}} + \rho_0\dot{\eta}\theta - \rho_0\dot{e} \geq 0 \tag{58}$$

By considering the rates appearing in the CPI (58), we can conclude that the internal energy is a thermodynamical potential (do not directely depend on time) depending primarily on the deformation gradient, the entropy, and the polarization, i.e. $e = \hat{e}(\boldsymbol{F}, \mathbb{P}, \eta, \ldots)$. Since the entropy is not a measurable quantity, the internal energy is replaced usually by the Helmholtz free energy using a Legendre transformation.

$$\psi = \sup_{\eta}\{e - \theta\eta\} \quad , \quad \Psi = \rho_0\psi \tag{59}$$

Above we defined Helmholtz free energy per unit refernce volume as Ψ. The version of the CPI in terms of Helmholtz free energy is obtained by inserting the partial Legendre transformation (59) into (58).

$$\rho_0\mathscr{D}_{loc} = [\boldsymbol{gP} + \boldsymbol{F}^{-T}(\mathbb{E}\otimes\mathbb{P})] : \dot{\boldsymbol{F}} + \mathbb{E}\cdot\dot{\mathbb{P}} - \rho_0\eta\dot{\theta} - \dot{\Psi} \geq 0 \tag{60}$$

Implying the functional dependence $\Psi = \hat{\Psi}(\boldsymbol{F}, \mathbb{P}, \theta, \ldots)$. From now on we will confine our consideration to isothermal processes ($\dot{\theta} = 0$). For those processes the constitutive material response will be thermodynamically consistent if only the CPI (60) with $\dot{\theta} = 0$ is verified.

$$\mathscr{D}_{loc} = [\boldsymbol{gP} + \boldsymbol{F}^{-T}(\mathbb{E}\otimes\mathbb{P})] : \dot{\boldsymbol{F}} + \mathbb{E}\cdot\dot{\mathbb{P}} - \dot{\Psi} \geq 0 \tag{61}$$

We observe that the CPI could be expressed in terms of electromechanical power $\mathscr{P}$ done on the domain under cosideration. The the dissipation $\mathscr{D}$ can be seen as the power subtracted by rate of energy storage $\dot{\Psi}$.

$$\mathscr{D}_{loc} = \mathscr{P} - \dot{\Psi} \geq 0 \tag{62}$$

We would like to use the last form of the CPI (61) to derive a thermodynamically consistent formulation of the constitutive equations based on the argumentation of Coleman & Noll. Being consistent with the principle of equipresence, we assume that the constitutive equations depend upon the same set of variables:

$$\Psi = \hat{\Psi}(\boldsymbol{g}, \boldsymbol{F}, \mathbb{P}, \mathfrak{Q}) \tag{63}$$

with $\mathfrak{Q}$ set of the histiry variablesemployed for the description of inelastic dissipative behaviour. The spatial metric $\boldsymbol{g}$ is needed to compute the deformation measures in different

configurations. Based on this assumption and putting the time derivative of free energy function into CPI.

$$\mathscr{D}_{loc} = [\boldsymbol{gP} + \boldsymbol{F}^{-T}(\mathbb{E} \otimes \mathbb{P}) - \partial_{\boldsymbol{F}}\Psi] : \dot{\boldsymbol{F}} + [\mathbb{E} - \partial_{\mathbb{P}}\Psi] \cdot \dot{\mathbb{P}} - \partial_{\boldsymbol{\mathfrak{Q}}}\Psi \cdot \dot{\boldsymbol{\mathfrak{Q}}} \geq 0 \tag{64}$$

Contending that the thermodynamic restriction should be fulfilled for an arbitrary rate of the deformation gradient $\boldsymbol{F}$ and of the polarization $\mathbb{P}$ we obtain the particular form of the constitutive equations

$$\begin{aligned} \boldsymbol{gP} &= \partial_{\boldsymbol{F}}\hat{\Psi}(\boldsymbol{g}, \boldsymbol{F}, \mathbb{P}, \boldsymbol{\mathfrak{Q}}) - \boldsymbol{F}^{-T}(\mathbb{E} \otimes \mathbb{P}) \\ \mathbb{E} &= \partial_{\mathbb{P}}\hat{\Psi}(\boldsymbol{g}, \boldsymbol{F}, \mathbb{P}, \boldsymbol{\mathfrak{Q}}) \end{aligned} \tag{65}$$

accompanied with a reduced form of dissipation.

$$\mathscr{D}^{red}_{loc} = \boldsymbol{\mathfrak{M}} \cdot \dot{\boldsymbol{\mathfrak{Q}}} \geq 0 \qquad with \qquad \boldsymbol{\mathfrak{M}} := -\partial_{\boldsymbol{\mathfrak{Q}}}\hat{\Psi}(\boldsymbol{g}, \boldsymbol{F}, \mathbb{P}, \boldsymbol{\mathfrak{Q}}) \tag{66}$$

Here $\{\boldsymbol{\mathfrak{M}}\}$ is thermodynamical forces conjugated to the $\{\boldsymbol{\mathfrak{M}}\}$ set. We consider in this work a formulation of the local constitutive material response based on a set of independent variables which have a geometric character. This is in agreement with the work of Rosato [21]. To this aim we will choose electric field $\mathbb{E}$ as the strain like variable. Thus we need to transform the Helmholtz free energy function Ψ to the mixed energy-enthalpy function ψ' through a partial Legendre transformation.

$$\Psi' = \inf_{\mathbb{P}}\{\Psi - \mathbb{E} \cdot \mathbb{P}\} \tag{67}$$

which inserted into

$$\begin{aligned} \mathscr{D}_{loc} &= \mathscr{P}' - \dot{\Psi}' \geq 0 \\ \mathscr{P}' &= \mathscr{P} - \frac{d}{dt}(\mathbb{E} \cdot \mathbb{P}) \end{aligned} \tag{68}$$

This will lead to the following constitutive equations.

$$\begin{aligned} \boldsymbol{gP} &= \partial_{\boldsymbol{F}}\hat{\Psi}'(\boldsymbol{g}, \boldsymbol{F}, \mathbb{E}, \boldsymbol{\mathfrak{Q}}) - \boldsymbol{F}^{-T}(\mathbb{E} \otimes \mathbb{P}) \\ \mathbb{P} &= -\partial_{\mathbb{E}}\hat{\Psi}'(\boldsymbol{g}, \boldsymbol{F}, \mathbb{E}, \boldsymbol{\mathfrak{Q}}) \\ \boldsymbol{\mathfrak{M}} &= -\partial_{\boldsymbol{\mathfrak{Q}}}\hat{\Psi}'(\boldsymbol{g}, \boldsymbol{F}, \mathbb{E}, \boldsymbol{\mathfrak{Q}}) \end{aligned} \tag{69}$$

This formulation of mixed energy-enthalpy function at hand gives us constitutive equation for the normal mechanical stress, however we have already reformulated our balance equations with maxwell stress and we would prefer to change constitutive equations to obtain total stress $\boldsymbol{P}^{tot}$ out of it. To this end we define an amended energy balance which takes into acount the electrostatic energy stored in the free space underlying the domain under consideration.

$$\rho_0\psi'_{amnd} = \rho_0\psi' + \rho_0 u^e \tag{70}$$

with $\rho_0 u^e$ electrostatic energy stored in the reference configuration derived from the true expression in the actual configuration.

$$\begin{aligned} \rho u^e &= -\tfrac{1}{2}\epsilon_0 \boldsymbol{g}^{-1} : (\mathbb{e} \otimes \mathbb{e}) \\ \rho_0 u^e &= J\rho u^e = -\tfrac{1}{2}J\epsilon_0 \boldsymbol{C}^{-1} : (\mathbb{E} \otimes \mathbb{E}) \end{aligned} \tag{71}$$

To be able to add electrostatic energy into the stored part of the energy in CPI we should compensate it by adding its rate to the power $\mathscr{P}'$. Using new definitions of power and stored energy the CPI reads

$$\begin{aligned} \mathscr{D}_{loc} &= \mathscr{P}'_{amnd} - \dot{\Psi}'_{amnd} \geq 0 \\ \mathscr{P}'_{amnd} &= \mathscr{P}' + \rho_0 \dot{u^e} \end{aligned} \tag{72}$$

We can indeed write the amended electro-mechanical power in terms of the total first Piola stress tensor $\boldsymbol{P}^{tot} = \boldsymbol{P} + \boldsymbol{P}^M$ and of the electric displacement $\mathbb{D}$. The CPI in terms of the amended quantities then will read

$$\mathscr{D}_{loc} = \mathscr{P}'_{amnd} - \dot{\Psi}'_{amnd} = \boldsymbol{g}\boldsymbol{P}^{tot} : \dot{\boldsymbol{F}} - \mathbb{D} \cdot \dot{\mathbb{E}} - \dot{\Psi}'_{amnd} \geq 0 \tag{73}$$

And finally the constitutive equations in terms of amended mixed energy-enthalpy function are as follows

$$\begin{aligned} \boldsymbol{g}\boldsymbol{P}^{tot} &= \partial_{\boldsymbol{F}} \hat{\Psi}'_{amnd}(\boldsymbol{g}, \boldsymbol{F}, \mathbb{E}, \mathfrak{Q}) \\ -\mathbb{D} &= \partial_{\mathbb{E}} \hat{\Psi}'_{amnd}(\boldsymbol{g}, \boldsymbol{F}, \mathbb{E}, \mathfrak{Q}) \\ \mathfrak{M} &= -\partial_{\mathfrak{Q}} \hat{\Psi}'_{amnd}(\boldsymbol{g}, \boldsymbol{F}, \mathbb{E}, \mathfrak{Q}) \end{aligned} \tag{74}$$

The constitutive equation (74) represent the starting point for our successive formulation which will take into account only the total stresses and the electric displacement. Once the field equations are solved, the Maxwell stress tensor and the polarization vector can be determined as post processing by using the proper definition.

In the following sections of this chapter we deal with elastic material and thus we will not consider the dependency of free energy function on $\mathfrak{Q}$. This variable will be used in the next chapter while formulating viscoelastic behaviour of the material. Moreover, for the sake of clarity we will not use anymore in the following the subscript *"amnd"* and the superscript *"tot"* and the *"prime"*.

3.2.1. Principle of Material Objectivity. In addition to the requirement of thermodynamic consistency discussed above, the constitutive equations must also satisfy the requirements of *material objectivity* and *material symmetry*. The *principle of material objectivity (PMO)*, also referred to as *principle of material frame-invariance*, requires that the material response be invariant under changes in observer (see e.g. Gurtin [7]). From the so-called *active viewpoint*, this requirement is equivalent to the statement that the energy stored in the system ought to be unaffected by rigid-body motions of the form $\boldsymbol{r}_t = \boldsymbol{Q}(t)\boldsymbol{x} + \boldsymbol{c}(t)$ superimposed onto the current configuration. Here, the proper orthogonal tensor $\boldsymbol{Q}(t) \in \mathcal{SO}(3)$ represents a time-dependent rotation and the vector $\boldsymbol{c}(t)$ a time-dependent translation. Consequently, the deformation gradient $\boldsymbol{F}^*$, which maps tangents to material curves onto tangents of the deformed and rigidly translated and rotated material curves, takes the form $\boldsymbol{F}^* = \boldsymbol{Q}\boldsymbol{F}$. The material electric field $\mathbb{E}$, however, is unaffected by observer transformations in the current configuration, since it is a Lagrangian field variable. For finite magnetoelasticity in the two-point setting, the amended free energy-enthalpy function $\Psi^* = \hat{\Psi}^*(\boldsymbol{F}, \boldsymbol{H})$ must therefore additionally comply with the constraint

$$\hat{\Psi}^*(\boldsymbol{F}^*, \mathbb{E}^*) = \hat{\Psi}^*(\boldsymbol{Q}\boldsymbol{F}, \mathbb{E}) \stackrel{!}{=} \hat{\Psi}^*(\boldsymbol{F}, \mathbb{E}) \ , \quad \forall\, \boldsymbol{Q} \in \mathcal{SO}(3) \ . \tag{75}$$

In order to satisfy the objectivity requirement *a priori*, one can introduce the *reduced form* of the free energy-enthalpy function.

$$\Psi^* = \hat{\Psi}^*(\boldsymbol{C}(\boldsymbol{F}), \mathbb{E}) = \hat{\Psi}^* \left(\boldsymbol{F}^T \boldsymbol{g} \boldsymbol{F}, \mathbb{E} \right) \ . \tag{76}$$

With the orthogonality relation $\boldsymbol{Q}^T\boldsymbol{g}\boldsymbol{Q}=\boldsymbol{g}$, it then directly follows

$$\begin{aligned}\hat{\Psi}^*(\boldsymbol{C}^*(\boldsymbol{F}^*),\mathbb{E}^*) &= \hat{\Psi}^*\left((\boldsymbol{F}^*)^T\boldsymbol{g}\boldsymbol{F}^*,\mathbb{E}\right) = \hat{\Psi}^*\left(\boldsymbol{F}^T\boldsymbol{Q}^T\boldsymbol{g}\boldsymbol{Q}\boldsymbol{F},\mathbb{E}\right)\\ &= \hat{\Psi}^*(\boldsymbol{F}^T\boldsymbol{g}\boldsymbol{F},\mathbb{E}) = \hat{\Psi}^*(\boldsymbol{C}(\boldsymbol{F}),\mathbb{E})\ .\end{aligned} \tag{77}$$

3.2.2. Material Symmetry. Textured and untextured poly-crystals, single-crystalline materials, many composites and also materials with imposed directions of polarization or magnetization exhibit symmetries in their microstructure that must be taken into account in the construction of constitutive models predicting their response. Furthermore, for dielectric elastomers, which, as discussed, are essentially consisting of an elastomeric material, we expect the response and thus the energy-enthalpy function to be independent of the sign of the electric field, i e.

$$\hat{\Psi}^*(\boldsymbol{C},\mathbb{E}) \stackrel{!}{=} \hat{\Psi}^*(\boldsymbol{C},-\mathbb{E})\ , \tag{78}$$

which is automatically satisfied if one assumes

$$\hat{\Psi}^*(\boldsymbol{C},\mathbb{E}) = \hat{\Psi}^*(\boldsymbol{C},\mathbb{E}\otimes\mathbb{E})\ . \tag{79}$$

The *principle of material symmetry* states that locally the free energy-enthalpy function ought to be invariant with respect to rotations $\boldsymbol{Q}$ superimposed onto the open neighborhood $\mathcal{N}_X\subset\mathcal{B}$ of a material point $\boldsymbol{X}$ in the reference configuration, in case these rotations are elements of the appropriate *material symmetry group* $\mathcal{G}\subset\mathcal{SO}(3)$. Or in other words, a electromechanical experiment involving the considered material should make no distinction between symmetry-related reference states. For the objective reduced form of the free energy-enthalpy function this requirement is mathematically expressed as

$$\hat{\Psi}^*(\boldsymbol{C}^*,\mathbb{E}^*) = \hat{\Psi}^*(\boldsymbol{Q}\boldsymbol{C}\boldsymbol{Q}^T,\boldsymbol{Q}\mathbb{E}) \stackrel{!}{=} \hat{\Psi}^*(\boldsymbol{C},\mathbb{E})\ ,\quad \forall\,\boldsymbol{Q}\in\mathcal{G}\subset\mathcal{SO}(3)\ . \tag{80}$$

Note that for an isotropic material the symmetry group is identical to the set of all rotations, i.e. $\mathcal{G}\equiv\mathcal{SO}(3)$. From the combination of (79) and (80), one thus demands that the free energy-enthalpy function, in order to satisfy objectivity, material symmetry and invariance with respect to the sign of the electric field, satisfy the following constraint

$$\hat{\Psi}^*\left(\boldsymbol{Q}\boldsymbol{C}\boldsymbol{Q}^T,\boldsymbol{Q}(\mathbb{E}\otimes\mathbb{E})\boldsymbol{Q}^T\right) \stackrel{!}{=} \hat{\Psi}^*(\boldsymbol{C},\mathbb{E}\otimes\mathbb{E})\ ,\quad \forall\,\boldsymbol{Q}\in\mathcal{G}\ . \tag{81}$$

3.3. Elastic Material Response Formulation

In this chapter we will focus on a non-dissipative electro mechanical response which implies a path independency of the work done to the material element. This can be expressed with a potential character of the electromechanical power. Using 73 we will obtain the following characteristic of $\mathscr{P}$.

$$\int_0^t \mathscr{P} = \hat{\Psi}(t) - \hat{\Psi}(0) \tag{82}$$

With $\hat{\Psi}(t)$ mixed energy-enthalpy stored in the system at time t. To this end $\hat{\Psi}(t)$ should only be a function of generalized covector.

$$\hat{\Psi}(t) = \Psi(\mathfrak{F}(t))\qquad,\qquad \mathfrak{S} = \partial_{\mathfrak{F}}\Psi(\mathfrak{F}) \tag{83}$$

In this work we assume an additive split of free enrgy-enthalpy functional into purely mechanical and electro-mechanical parts

$$\Psi(\mathfrak{F}(t)) = \Psi_{mech}(\boldsymbol{F}) + \Psi_{elem}(\boldsymbol{F}, \mathbb{E}) \tag{84}$$

In which $\hat{\Psi}_{mech}(\boldsymbol{F})$ is a purely mechanical free energy function and $\hat{\Psi}_{elem}(\boldsymbol{F}, \mathbb{E})$ is the electro-mechanical free energy-enthalpy function.

The electro-mechanical stress power per unit of reference volume could be written alternatively in terms of the second Piola-Kirchhoff stress $\boldsymbol{S}$ and the rate of the Cauchy-Green tensor $\boldsymbol{C}$.

$$\mathscr{P} = \boldsymbol{gP} : \dot{\boldsymbol{F}} - \mathbb{D} \cdot \dot{\mathbb{E}} = \boldsymbol{S} : \frac{1}{2}\dot{\boldsymbol{C}} - \mathbb{D} \cdot \dot{\mathbb{E}} \tag{85}$$

Thus, we could define the set of constitutive equations in terms of a free energy functions with dependence on Cauchy-Green tensor $\psi = \tilde{\psi}(\boldsymbol{C}, \mathbb{E})$. This will ensure objectivity in the material response.

$$\boldsymbol{S} = 2\partial_{\boldsymbol{C}}\Psi(\boldsymbol{C}, \mathbb{E}) \qquad , \qquad -\mathbb{D} = \partial_{\mathbb{E}}\Psi_{elem}(\boldsymbol{C}, \mathbb{E}) \tag{86}$$

Elastomers show a completely decoupled response over any range of volumetric and deviatoric deformation. This is achived by by a local multiplicative decomposition of the deformation gradient into volumetric and dialational parts. One can find this approach in the works of Lubliner [12] and Simo [23] among others.
Let $J = det(\boldsymbol{F})$ to be Jacobian of the deformation gradient. To properly define volumetric and deviatoric response in the nonlinear regime we introduce the following kinematic split:

$$\boldsymbol{F} = J^{1/3}\bar{\boldsymbol{F}} \qquad \text{where} \qquad \bar{\boldsymbol{F}} = J^{-1/3}\boldsymbol{F} \tag{87}$$

Since $det\bar{\boldsymbol{F}} = 1$, we refer to $\bar{\boldsymbol{F}}$ as the *volume preserving* part of the deformation gradient $\boldsymbol{F}$. Associated with $\boldsymbol{F}$ and $\bar{\boldsymbol{F}}$ we defime the corrsponding right Cauchy-Green tensors as:

$$\boldsymbol{C} = \boldsymbol{F}^T\boldsymbol{gF} \qquad , \qquad \bar{\boldsymbol{C}} = J^{-2/3}\boldsymbol{C} = \bar{\boldsymbol{F}}^T\boldsymbol{g}\bar{\boldsymbol{F}} \tag{88}$$

Using this decomposition and considering independent volumetric and deviatoric response of rubber materials one can propose an additive decomposition of the mechanical part of the free enegy-enthalpy function into volumetric and deviatoric strain energies.

$$\Psi(\mathfrak{F}(t)) = \Psi_{mech}(\boldsymbol{C}) + \Psi_{elem}(\boldsymbol{C}, \mathbb{E}) = \Psi^{\infty}_{vol}(J) + \Psi^{\infty}_{iso}(\bar{\boldsymbol{C}}) + \Psi_{elem}(\boldsymbol{C}, \mathbb{E}) \tag{89}$$

Here, $\Psi^{\infty}_{vol}(J)$ is a fully convex function describing the stored energy due to volume changes and $\Psi^{\infty}_{iso}(\bar{\boldsymbol{C}})$ is a poly convex function giving the elastic energy of the deviatoric deformation. Furthermore, if we assume isotropic material response, we can express the free energy as a function of invariants of Cauchy-Green tensor. $\Psi^{\infty}_{vol}(J)$ characterizes the dependence on the third invariant of the right Cauchy-Green tensor. Thus $\Psi^{\infty}_{iso}(\bar{\boldsymbol{C}})$ should be expressed in tems of the first and second invariants of $\bar{\boldsymbol{C}}$.

Many of common rubber material models such as Arrunda-Boyce and Neo-Hooke materials use only the first invariant $I_{\bar{\boldsymbol{C}}}$ of the deviatoric Cauchy-Green tensor to characterize

deviatoric part of the response(see KALISKE & ROTHERT [11]). We will consider this type of free enegy function in this work.

$$\Psi(\mathfrak{F}(t)) = \Psi^{\infty}_{vol}(J) + \Psi^{\infty}_{iso}(I_{\bar{\boldsymbol{C}}}) + \Psi_{elem}(\boldsymbol{C}, \mathbb{E}) \tag{90}$$

In our approach, rubber material is considered as being slightly compressible or nearly incompressible. This assumption is valid for most types of rubber in technical applications. This way, a volumetric strain energy function and, therefore, a slight volumetric deformation can be motivated.

$$\Psi^{\infty}_{vol}(J) = \frac{\kappa}{2}\left(\frac{J^2-1}{2} - \ln J\right) \tag{91}$$

Which is for example used by KALISKE & ROTHERT [11]. κ is the material volumetric modulus. Due to the poisson's ratio of rubbers which is near to 0.5, the volumetric modulus is bigger from material shear modulus by some order of magnitude. Thus, usually material does not show big volumetric deformations.
Based on an eight-chain representation of the macromolecular network structure and non-Gaussian behavior of the polymer chains, ARRUDA & BOYCE [1] proposed a constitutive rubber model. This potential function formulated in the first invariant of $\bar{\boldsymbol{C}}$ depends on two material parameters: the shear modulus μ and N which can be interpreted as measure of the limiting network stretch.

$$\begin{aligned}\Psi^{\infty}_{iso}(I_{\bar{\boldsymbol{C}}}) &= \mu[\frac{1}{2}\left(I_{\bar{\boldsymbol{C}}}-3\right) + \frac{1}{20N}\left(I^2_{\bar{\boldsymbol{C}}}-9\right) + \frac{1}{1050N^2}\left(I^3_{\bar{\boldsymbol{C}}}-27\right) \\ &\quad + \frac{1}{7000N^3}\left(I^4_{\bar{\boldsymbol{C}}}-81\right) + \frac{1}{673750N^4}\left(I^5_{\bar{\boldsymbol{C}}}-243\right)]\end{aligned} \tag{92}$$

3.4. Electrical Material Response Formulation

Many experiments suggest that for dielectric elastomers, the true electric displacement is linear in the true electric field, i.e. $\mathbb{d} = \epsilon \mathbb{e}$, with the permittivity being approximately independent of the state of deformation (PLANTE & DUBOWSKY [19]).
This experimental observations could be interpreted as follows. Each polymer in an elastomer is a long chain of covalently bonded links. The neighboring links along the chain can readily rotate relative to each other, so that the chain is flexible. A link also interacts with links on other chains through weak bonds. Different chains are cross-linked with covalent bonds to form a three-dimensional network. When each chain contains a large number of links and when the end-to-end distance of the chain has not reached its fully stretched length, the extension limit, the local behavior of the links is just like molecules in a liquid. The elastomer can polarize nearly as freely as in liquids. Furthermore, for an elastomer with an approximately isotropic dielectric behavior, we surmise that the polarizability of links is comparable in the directions along the chain and transverse to the chain(ZHAO ET.AL. [27]).
The free energy of the liquid polymer per unit current volume is $\mathbb{d}\cdot\mathbb{d}/2\epsilon$ and it can be written as energy per unit reference volume.

$$\Psi_{elec}(\mathbb{d}) = \frac{dv}{dV}\frac{\mathbb{d}\cdot\mathbb{d}}{2\epsilon} = J\frac{\mathbb{d}\cdot\mathbb{d}}{2\epsilon} = J\frac{\mathbb{e}\cdot\mathbb{d}}{2} \tag{93}$$

By a pull back operation on $\mathbb{d}$ and $\mathbb{e}$, we can rewrite above energy function in the following form.

$$\Psi_{elec}(\mathbb{d}) = J\frac{F^{-T}\mathbb{E}\cdot J^{-1}F\mathbb{D}}{2} = \frac{\mathbb{E}\cdot\mathbb{D}}{2} \tag{94}$$

To obtain mixed energy enthalpy the Legendre transformation is used to transform electric displacement dependent function to electric field dependent function.

$$\Psi_{elem}(\mathbb{E}) = \inf_{\mathbb{D}}\{\psi_{elec}(\mathbb{E}) - \mathbb{E}\cdot\mathbb{D}\} = -\frac{\mathbb{E}\cdot\mathbb{D}}{2} \tag{95}$$

Pushing forward 95 and using true form of electrical material law and pulling it back again will end up with the electromechanical term of the mixed free energy enthalpy.

$$\begin{aligned} \Psi_{elem}(\mathbb{e}) &= -\frac{F^T\mathbb{e}\cdot JF^{-1}\mathbb{d}}{2} = -J\frac{\mathbb{e}\cdot\epsilon\mathbb{e}}{2} \\ \Psi_{elem}(\mathbb{E}) &= -J\epsilon\frac{F^{-T}\mathbb{E}\cdot F^{-T}\mathbb{E}}{2} = -J\epsilon\frac{C^{-1}:(\mathbb{E}\otimes\mathbb{E})}{2} \end{aligned} \tag{96}$$

This formulation has the energy of underlying space in it, because $\mathbb{d}$ composed of both polarization of the material and the underlying space electric displacement. Furthermore, this formula shows the dependence of electromechanical energy on right Cauchy-Green tensor that ensures objectivity.

4. Finite Electro Visco Elasticity

In this chapter we will present the viscoelastic material modeling at large strain. This derivation includes the the typical steps of defining the finite deformation viscoelasticity. We will start with free energy function which is established in the previous chapter for elasticity and extend it for viscoelastic case. Rate equation as well as numerical treatment will be covered.

Several formulations of non-linear viscoelastic models have been published in the recent years. Lubliner [12] as one of the pioneering researches, proposed a model based on the multiplicative decomposition of the deformation of the deformation gradient into elastic and viscoelastic component. The resulting model is only limited by choice of linear rate equations to describe the relaxation of viscoelastic stresses. Simo [23], Govindjee & Simo [6] and Holzapfel [8] have proposed alternative models in which the evolution equation of the viscous overstress is defined directly by a linear differential equation motivated by small strain case. The nonequlibrium overstress mimics the force relaxation process taking place in linear rheological models. In this work we will use this approach to tackle the problem of large strain viscoelastic effects in Electroactive Polymers.

4.1. Free Mixed Energy Enthalpy Function for Viscoelasticity

Our discussion will be based on theory of compressible hyperelasticity within the isothermal regime. As discussed in section (3.3), we postulate a decoupled representation of the Helmholtz free energy function for the mechanical part. The free energy uses the multiplicative decomposition of the form represented in equation (87). Adding effect of internal variables to the free energy function (89) we can modify it as follows.

$$\Psi(\mathfrak{F}(t)) = \Psi^{\infty}_{vol}(J) + \Psi^{\infty}_{iso}(\bar{\boldsymbol{C}}) + \sum_{\alpha} \Upsilon_{\alpha}(\bar{\boldsymbol{C}}, \boldsymbol{\Gamma}_{\alpha}) + \Psi_{elem}(\boldsymbol{C}, \mathbb{E}) \tag{97}$$

where $\boldsymbol{\Gamma}_{\alpha}(\alpha = 1, ..., m)$ are a set of (non-measurable) internal variables. Each α is regarded as a strain tensor analogous to the symmetric strain tensor $\bar{\boldsymbol{C}}$. The relaxational behavior is modeled by $m > 1$ relaxation processes with corresponding relaxation times $\tau_{\alpha} \in (0, \inf)$. Motivated by experimental data we assume a time-dependent change in the free energy only due to isochoric deformations; hence, the volumetric response is fully elastic. The first two terms are strain energy functions per unit reference volume and characterize the *volumetric* ($\Psi^{\infty}_{vol}(J)$) and *isochoric* ($\Psi^{\infty}_{iso}(\bar{\boldsymbol{C}})$) elastic response as $t \to \infty$. The superscript $[\cdot]^{\infty}$ characterizes functions which represent the hyperelastic behaviour of very slow processes. Last term is the *electromechanical* ($\Psi_{elem}(\boldsymbol{C}, \mathbb{E})$) response. This term is considered to be purely elastic.

4.1.1. Stress Response. One form of the second law of thermodynamics is the Clausius-Plank inequality, which for isothermal electromechanical process reads:

$$\mathscr{D}_{loc} = \boldsymbol{S} : \frac{1}{2}\dot{\boldsymbol{C}} - \mathbb{D} \cdot \dot{\mathbb{E}} - \dot{\Psi} \geq 0 \tag{98}$$

A particularization of (98) to the constitutive model at hand is obtained by time differentiation of (97) using the chain rule, we obtain

$$\mathscr{D}_{loc} = (\boldsymbol{S} - 2\partial_{\boldsymbol{C}}\Psi) : \frac{1}{2}\dot{\boldsymbol{C}} - (\mathbb{D} + \partial_{\mathbb{E}}\Psi) : \dot{\mathbb{E}} - \sum_{\alpha} \partial_{\boldsymbol{\Gamma}_{\alpha}}\Psi : \dot{\boldsymbol{\Gamma}}_{\alpha} \geq 0 \tag{99}$$

This yields the fundamental constitutive hyperelastic equation for the convected stresses $\boldsymbol{S}$, $\mathbb{D}$ and a remainder inequality for the dissipation:

$$\boldsymbol{S} = 2\partial_{\boldsymbol{C}}\Psi(\boldsymbol{C},\mathbb{E}) \quad , \quad -\mathbb{D} = \partial_{\mathbb{E}}\Psi_{elem}(\boldsymbol{C},\mathbb{E}), \quad \mathscr{D}_{loc} = -\sum_{\alpha}\partial_{\boldsymbol{\Gamma}_\alpha}\Upsilon_\alpha : \dot{\boldsymbol{\Gamma}}_\alpha \geq 0 \quad (100)$$

Starting from a decoupled free energy enthalpy function leads to an additive split of $\boldsymbol{S}$ into volumetric and isochoric and electromechanical parts. The electric displacement is not effected by viscous energy term and will be the same as elastic case.

$$\boldsymbol{S} = \boldsymbol{S}^{\infty}_{vol} + \boldsymbol{S}_{iso} + \boldsymbol{S}_{elem} \qquad \text{with} \qquad \boldsymbol{S}_{iso} = \boldsymbol{S}^{\infty}_{iso} + \sum_{\alpha}\boldsymbol{Q}_\alpha \tag{101}$$

To proceed we need the following derivatives to take the derivatives of the free energy enthalpy function.

$$\partial_{\boldsymbol{C}}(\det\boldsymbol{C}) = (\det\boldsymbol{C})\boldsymbol{C}^{-T} \quad , \quad \partial_{\boldsymbol{C}}\bar{\boldsymbol{C}} = J^{-2/3}(\mathbb{I} - \frac{1}{3}\boldsymbol{C}\otimes\boldsymbol{C}^{-1}) \tag{102}$$

Here, $\mathbb{I}$ is the forth order identity tensor. The expression $\mathbb{I}-\frac{1}{3}\boldsymbol{C}^{-1}\otimes\boldsymbol{C}$ can be interpreted as a forth order projection tensor which furnishes the physically correct deviator in material description[8]. We define the deviatoric projector $\mathbb{P}$ as:

$$\mathbb{P} = \mathbb{I} - \frac{1}{3}\boldsymbol{C}^{-1}\otimes\boldsymbol{C} \quad , \quad \partial_{\boldsymbol{C}}\bar{\boldsymbol{C}} = J^{-2/3}\mathbb{P}^T \tag{103}$$

Using the derivatives (102), we can obtain the quantities which are defined in (101). First we derive the electromechanical and volumetric part.

$$\boldsymbol{S}^{\infty}_{vol} = J\frac{\mathrm{d}\Psi^{\infty}_{vol}(J)}{\mathrm{d}J}\boldsymbol{C}^{-1}, \qquad \boldsymbol{S}_{elem} = 2\frac{\partial\Psi_{elem}(\boldsymbol{C},\mathbb{E})}{\partial\boldsymbol{C}} \tag{104}$$

The electromechanical and volumetric part of the stress is quite straight forward and will not need further attention. However, we focus on the isochoric part of it. In equation (101) we have also a *nonequilibrium stress* which also should be taken into account. As can be seen the isochoric second Piola-Kirchhoff is:

$$\begin{aligned} \boldsymbol{S}^{\infty}_{iso} &= J^{-2/3}\mathbb{P} : \bar{\boldsymbol{S}}^{\infty}_{iso}, \qquad \text{with} \quad \bar{\boldsymbol{S}}^{\infty}_{iso} = 2\frac{\partial\Psi^{\infty}_{iso}(\bar{\boldsymbol{C}},\mathbb{E})}{\partial\bar{\boldsymbol{C}}} \\ \boldsymbol{Q}_\alpha &= J^{-2/3}\mathbb{P} : \bar{\boldsymbol{Q}}_\alpha, \qquad \text{with} \quad \bar{\boldsymbol{Q}}_\alpha = 2\frac{\partial\Upsilon_\alpha(\bar{\boldsymbol{C}},\mathbb{E})}{\partial\bar{\boldsymbol{C}}} \end{aligned} \tag{105}$$

As mentioned before the projector tensor $\mathbb{P}$ will ensure that we have a deviatoric tensor in the material description. In other words:

$$\boldsymbol{S}^{\infty}_{iso} = J^{-2/3}\mathbb{P} : \bar{\boldsymbol{S}}^{\infty}_{iso} = J^{-2/3}\mathrm{Dev}\left[\bar{\boldsymbol{S}}^{\infty}_{iso}\right], \qquad \boldsymbol{Q}_\alpha = J^{-2/3}\mathbb{P} : \bar{\boldsymbol{Q}}_\alpha = J^{-2/3}\mathrm{Dev}\left[\bar{\boldsymbol{Q}}_\alpha\right] \tag{106}$$

Using mixed energy enthalpy function defined in previous chapter and equations (100-105) one obtains following Second Piola-Kirchhoff stresses and lectrical displacement.

$$\begin{aligned} \boldsymbol{S}^{\infty}_{vol} &:= 2\partial_{\boldsymbol{C}}\Psi^{\infty}_{vol} &&= Jp\boldsymbol{C}^{-1} \\ \boldsymbol{S}^{\infty}_{iso} &:= 2\partial_{\boldsymbol{C}}\Psi^{\infty}_{iso} &&= 2J^{-2/3}\mathbb{P} : \sigma\boldsymbol{I} \\ \boldsymbol{S}_{elem} &:= 2\partial_{\boldsymbol{C}}\Psi_{elem} &&= \frac{\epsilon J}{2}[\boldsymbol{C}^{-1} : (\mathbb{E}\otimes\mathbb{E})]\boldsymbol{C}^{-1} - \epsilon J[\boldsymbol{C}^{-T}\mathbb{E}\otimes\boldsymbol{C}^{-T}\mathbb{E}] \\ -\mathbb{D} &:= \partial_{\mathbb{E}}\Psi_{elem} &&= -\epsilon J\boldsymbol{C}^{-T}\mathbb{E} \end{aligned} \tag{107}$$

In which

$$\begin{aligned} p &:= \partial_J \Psi^{\infty}_{vol}(J) \\ \sigma &:= \partial_{I_{\bar{\boldsymbol{C}}}} \Psi^{\infty}_{iso}(I_{\bar{\boldsymbol{C}}}) \end{aligned} \tag{108}$$

As we will use a finite element formulation based on a two-point setting i.e. $\{\boldsymbol{P}, \boldsymbol{F}\}$, we should find corresponding stress which is first Piola-Kirchhoff stress $\boldsymbol{P}$. Using the definitions given in section (2.2) we will use bellow mapping for mechanical stresses to obtain appropriate output for the finite element formulation.

$$\boldsymbol{P} = \boldsymbol{F}\boldsymbol{S} \tag{109}$$

4.2. Evolution Equation

Motivated by the standard linear solid we define $\boldsymbol{Q}_\alpha$ to be variables conjugate to $\boldsymbol{\Gamma}_\alpha$ with constitutive relation $\boldsymbol{Q}_\alpha = -\partial_{\boldsymbol{\Gamma}_\alpha} \Upsilon_\alpha(\bar{\boldsymbol{C}}, \boldsymbol{\Gamma}_\alpha)$. With that in mind, the local entropy production is governed by relation

$$\mathscr{D}_{loc} = -\sum_{\alpha} \boldsymbol{Q}_\alpha : \boldsymbol{\Gamma}_\alpha \tag{110}$$

Equation (110) as a form of Clausius-Planck inequality is satisfied by specifying a suitable evolution equation for the internal strains such as:

$$\dot{\boldsymbol{\Gamma}}_\alpha = \mathbb{V}(\bar{\boldsymbol{C}}, \boldsymbol{\Gamma}_\alpha) : \boldsymbol{Q}_\alpha \tag{111}$$

Where $\mathbb{V}(\bar{\boldsymbol{C}}, \boldsymbol{\Gamma}_\alpha)$ is a fourth order positive definite tensor which contains the inverse viscosity. A relaxation process involves a trend to equilibrium in a mechanical systemwhich is attained in the limit of infinite time. This notion can be recast in mathematical term by assigning $\boldsymbol{Q}_\alpha$, which is governed by a dissipative evolution equation. Furthermore, motivated by small strain viscoelasticity combining equation (111) with a linear evolution equation for internal strain-like varibles will end up with a linear dissipative evolution equation for $\boldsymbol{Q}_\alpha$. The over-stress should be regarded as a convected stress tensor akin to the second Piola-Kirchhoff stress. This will perclude restriction to frame invariance. Moreover, to maintain a materially deviatoric stress tensor we write the dissipative evolution equation for $\bar{\boldsymbol{Q}}_\alpha$ instead of $\boldsymbol{Q}_\alpha$(see e.g. Govindjee & Simo [6]). Thus the simmplest appropraite dissipative evolution equation reads:

$$\dot{\bar{\boldsymbol{Q}}}_\alpha + \frac{\bar{\boldsymbol{Q}}_\alpha}{\tau_\alpha} = \frac{\mathrm{d}}{\mathrm{ds}} \left[\mathbb{P} : 2\partial_{\bar{\boldsymbol{C}}} \Psi_\alpha(\bar{\boldsymbol{C}}) \right], \qquad \bar{\boldsymbol{Q}}_\alpha|_{t=0} = \bar{\boldsymbol{Q}}_\alpha|^0 \tag{112}$$

In (112) Ψ^α is a function denoting the free energy of the body, which corresponds to the α-relaxation process with relaxation time $\tau_\alpha > 0$. Since the phenomenological relaxation effect is induced by a viscous environment induced by identical polymer chains, it will be assumed that:

$$\Psi_\alpha(\bar{\boldsymbol{C}}) = \beta_\alpha \Psi^{\infty}_{iso}(\bar{\boldsymbol{C}}), \qquad (\alpha = 1, ..., m) \tag{113}$$

Herein $\beta_\alpha \in (0, \infty)$ is the free energy factor associated with $\tau_\alpha > 0$. Furthermore if we use the neutral state as the begining step ($t = 0$), the value of $\bar{\boldsymbol{Q}}_\alpha|_{t=0}$ which is the viscous stress at this time ($\mathbb{P}|_{t=0} = \mathbb{I} \rightarrow \boldsymbol{Q}^0_\alpha = \bar{\boldsymbol{Q}}^0_\alpha$) considered to be zero. In other words, equation

(112) suggeste a dissipative evolution of nondeviatoric overstress $\bar{\boldsymbol{Q}}_\alpha$ driven by deviatoric elastic stress $J^{-2/3}\mathbb{P} : 2\partial_{\bar{\boldsymbol{C}}}\Psi^{\infty}_{iso}(\bar{\boldsymbol{C}})$ multiplied by a free energy factor β_α. Assumption (113) along with the dissipative evolution equation (112) help us to exclude viscoelastic part of the free energy function in proceeding formulation. Using the integrating factor $exp(s/\tau_\alpha)$, one obtains the explicit solution to the evolution equation as:

$$\bar{\boldsymbol{Q}}^t_\alpha = exp[-t/\tau_\alpha]\bar{\boldsymbol{Q}}^0_\alpha + \int_{0^+}^{t} \beta_\alpha exp[-(t-s)/\tau_\alpha]\frac{\mathrm{d}}{\mathrm{ds}}\left[\mathbb{P} : 2\partial_{\bar{\boldsymbol{C}}}\Psi^{\infty}_{iso}(\bar{\boldsymbol{C}})\right]\mathrm{ds} \tag{114}$$

4.3. Time Integration Algorithm

The main goal of this section is to outline an update algorithm for the stress tensor and the consistent material tangent, which are required for the solution of the balance laws within an iterative technique. The numerical integration is related to the approach introduced by Simo [23], which bypasses the need for incremental objectivity.

4.3.1. Algorithmic Update for Stress and Electric Displacement. Consider a partition $\bigcup_{n=0}^{M}[t_n, t_{n+1}]$ of the time interval $[0^+, T]$ of interest, where $0^+ = t_0 < t_{M+1} = T$, and let us focus attention on a typical time subinterval $[t_n, t_{n+1}]$, with $\Delta t := t_{n+1} - t_n \in \mathbb{R}^+$ characterizing the associated time increments.

Assume that up to a certain time t_n the stresses satisfy equilibrium and that the stresses $\boldsymbol{S}_n$, and the strain measures $\boldsymbol{F}_n, \boldsymbol{C}_n$ are uniquely specified from the known motion $\boldsymbol{\varphi}_n(\boldsymbol{X}, t_n)$. To advance the solution to time t_{n+1} we first make an initial guess for $\boldsymbol{\varphi}_{n+1}$ and update the prescribed loads. Within a classical Newton-Raphson method the new configuration is iteratively corrected until the balance laws of momentum are satisfied within a given tolerance of accuracy. To check equilibrium at time t_{n+l}, all relevant strain measures and the equilibrium stresses have to be computed via previous given relations, respectively, which is straightforward, since $\boldsymbol{\varphi}_{n+1}$ is regarded as given[8].

In addition to these continuum variables the viscoelastic stress contribution $\boldsymbol{Q}_n$ must be evaluated. To do this we split the convolution integral given in (114) into the form $\int_{0^+}^{t_{n+1}}(\cdot)ds = \int_{0^+}^{t_n}(\cdot)ds + \int_{t_n}^{t_{n+1}}(\cdot)ds$. The internal variable at t_{n+l} is recovered by using the second-order accurate midpoint rule on the $\int_{t_n}^{t_{n+1}}(\cdot)ds$ term. After some algebraic manipulations one obtains:

$$\begin{aligned}
\bar{\boldsymbol{Q}}^{n+1}_\alpha &= exp[-\Delta t/\tau_\alpha]\bar{\boldsymbol{Q}}^n_\alpha + \int_{t_n}^{t_{n+1}} \beta_\alpha exp[-(t_{n+1}-s)/\tau_\alpha]\frac{\mathrm{d}}{\mathrm{ds}}(J^{2/3}\bar{\boldsymbol{S}}^{\infty}_{iso})\mathrm{ds} \\
&= exp[-\Delta t/\tau_\alpha]\bar{\boldsymbol{Q}}^n_\alpha \\
&+ \beta_\alpha exp[-(t_{n+1} - \frac{t_{n+1}+t_n}{2})/\tau_\alpha]\left(J^{n+1\,2/3}\bar{\boldsymbol{S}}^{\infty,n+1}_{iso} - J^{n\,2/3}\bar{\boldsymbol{S}}^{\infty,n}_{iso}\right) \\
&= exp[-\Delta t/\tau_\alpha]\bar{\boldsymbol{Q}}^n_\alpha \\
&+ \beta_\alpha exp[-\Delta t/2\tau_\alpha]J^{n+1\,2/3}\bar{\boldsymbol{S}}^{\infty,n+1}_{iso} - \beta_\alpha exp[-\Delta t/2\tau_\alpha]J^{n\,2/3}\bar{\boldsymbol{S}}^{\infty,n}_{iso}
\end{aligned} \tag{115}$$

This can be defined in terms of algorithmic history variables $\bar{\boldsymbol{\mathcal{H}}}^\alpha$ as follows:

$$\begin{aligned}
\bar{\boldsymbol{Q}}^{n+1}_\alpha &= \beta_\alpha exp[-\Delta t/2\tau_\alpha]J^{n+1\,2/3}\bar{\boldsymbol{S}}^{\infty,n+1}_{iso} + \bar{\boldsymbol{\mathcal{H}}}^{\alpha,n} \\
\text{with}\quad \bar{\boldsymbol{\mathcal{H}}}^{\alpha,n} &= exp[-\Delta t/\tau_\alpha]\bar{\boldsymbol{Q}}^n_\alpha - \beta_\alpha exp[-\Delta t/2\tau_\alpha]J^{n\,2/3}\bar{\boldsymbol{S}}^{\infty,n}_{iso}
\end{aligned} \tag{116}$$

Using a constitutive model which were described in the previous chapter and the FE method the algorithmic update on the principal values at each Gauss point of a finite element can be carried out. Summary of numerical update proceedure is reflected in Box (1).

4.3.2. Consistent Tangent in Material Setting. To obtain the solution of the non-linear BVP an incremental iterative process of Newton's type is applied, which solves a sequence of linearized problems. This strategy requires knowledge of the tangent moduli which have to be specified within an exact linearization procedure[9]. Consistent linearized moduli are crucial in preserving the quadratic rate of convergence near the solution point in Newton methods. Consequently, providing the closed-form moduli is an important task and is the goal of this section. The generalized moduli is the derivative of generalized stress with respest to generalized strain. $\mathfrak{C} = \partial_{\mathfrak{F}}\mathfrak{S}$. As we worked with the material description parameters here, we should calculate the mapping between the material description of the moduli $\mathfrak{C}$ and the two-point description of it $\mathfrak{C}$ which is needed for the finite element formulation. To this end we will first introduce the material description $\mathfrak{C}$ and the two-point description of the moduli.

$$\mathfrak{C} := \begin{bmatrix} \boldsymbol{\mathcal{C}} & \mathfrak{h} \\ \mathfrak{h}^T & \boldsymbol{\beta} \end{bmatrix} = \begin{bmatrix} \partial_{\boldsymbol{F}}(\boldsymbol{gP}) & \partial_{\mathbb{E}}(\boldsymbol{gP}) \\ \partial_{\boldsymbol{F}}(-\mathbb{D}) & \partial_{\mathbb{E}}(-\mathbb{D}) \end{bmatrix}, \qquad \mathfrak{C} := \begin{bmatrix} \mathbb{C} & \boldsymbol{h} \\ \boldsymbol{h}^T & \boldsymbol{\beta} \end{bmatrix} = \begin{bmatrix} 2\partial_{\boldsymbol{C}}\boldsymbol{S} & \partial_{\mathbb{E}}\boldsymbol{S} \\ \partial_{\boldsymbol{C}}(-\mathbb{D}) & \partial_{\mathbb{E}}(-\mathbb{D}) \end{bmatrix} \tag{117}$$

The desired mapping can be shown to be as following.

$$\begin{aligned} \boldsymbol{\mathcal{C}}_a{}^A{}_b{}^B &= \delta_{ab}S^{BA} + g_{ac}F^c{}_C\,\mathbb{C}^{CADB}F^d{}_D\,g_{bd} \\ \mathfrak{h}_a{}^{AB} &= g_{ac}F^c{}_C\,h^{CAB} \end{aligned} \tag{118}$$

Considering different parts of stress tensor in equation (101), one can easily obtain the same terms for the mechanical part of the moduli:

$$\mathbb{C}^{n+1} = 2\partial_{\boldsymbol{C}}\boldsymbol{S}^{n+1} = [\mathbb{C}^{\infty}_{vol} + \mathbb{C}^{\infty}_{iso} + \sum_{\alpha}\mathbb{C}^{\alpha}_{vis} + \mathbb{C}_{elem}]|^{n+1} \tag{119}$$

To obtain the moduli the derivative (120) is needed. For the sake of simplicity an abbreviation is defined.

$$\partial_{\boldsymbol{C}}(\boldsymbol{C}^{-1}) = -(\boldsymbol{C}^{-1}\odot\boldsymbol{C}^{-1}) \qquad \text{with} \qquad (\boldsymbol{C}^{-1}\odot\boldsymbol{C}^{-1})_{ABCD} = \frac{1}{2}(C^{-1}_{AC}C^{-1}_{DB} + C^{-1}_{AD}C^{-1}_{CB}) \tag{120}$$

The four component of $\boldsymbol{C}^{n+1}$ can be computed using free energy function defined in previous chapter, stress defined in section (4.1.1) and viscouse stress as a result of evolution equation (116).

- *Volumetric elastic part* which is denoted as $\mathbb{C}^{\infty}_{vol}$ is computed as:

$$\begin{aligned} \mathbb{C}^{\infty,n+1}_{vol} &:= 2\partial_{\boldsymbol{C}}\boldsymbol{S}^{n+1}_{vol} \\ &= \{J(p + J\frac{\partial p}{\partial J})\boldsymbol{C}^{-1}\otimes\boldsymbol{C}^{-1} - 2Jp\boldsymbol{C}^{-1}\odot\boldsymbol{C}^{-1}\}|^{n+1} \end{aligned} \tag{121}$$

  In which internal pressure is defined as the derivative of volumetric part of free energy $p = \partial\Psi^{\infty}_{vol}(J)/\partial J$.

- *Isochoric elastic contribution* which is denoted as $\mathbb{C}^{\infty}_{iso}$ and can be computed within some simple tensor calculation steps as:

$$\begin{aligned} \mathbb{C}^{\infty}_{iso} &:= 2\partial_{\boldsymbol{C}} \boldsymbol{S}^{n+1}_{iso} \\ &= \{J(p + J\frac{\partial p}{\partial J})\boldsymbol{C}^{-1} \otimes \boldsymbol{C}^{-1} - 2Jp\boldsymbol{C}^{-1} \odot \boldsymbol{C}^{-1}\}|^{n+1} \end{aligned} \tag{122}$$

- *Viscoelastic part* which is denoted as $\mathbb{C}^{\alpha}_{vis}$ is computed as:

$$\begin{aligned} \mathbb{C}_{vis} &:= 2\partial_{\boldsymbol{C}} \boldsymbol{Q}^{\alpha,n+1} \\ &= \{J(p + J\frac{\partial p}{\partial J})\boldsymbol{C}^{-1} \otimes \boldsymbol{C}^{-1} - 2Jp\boldsymbol{C}^{-1} \odot \boldsymbol{C}^{-1}\}|^{n+1} \end{aligned} \tag{123}$$

- *Volumetric elastic part* which is denoted as $\mathbb{C}_{elem}$ is computed as:

$$\begin{aligned} \mathbb{C}_{elem} &:= 2\partial_{\boldsymbol{C}} \boldsymbol{S}^{n+1}_{elem} \\ &= \{J(p + J\frac{\partial p}{\partial J})\boldsymbol{C}^{-1} \otimes \boldsymbol{C}^{-1} - 2Jp\boldsymbol{C}^{-1} \odot \boldsymbol{C}^{-1}\}|^{n+1} \end{aligned} \tag{124}$$

Box 2: Summary of update algorithm for the second Piola-Kirchhoff stresses and electrical displacement in material description.

1. Given *initial* data base at Gauss point.

$$\boldsymbol{F}^{n+1}\,,\mathbb{E}^{n+1}\,,\bar{\boldsymbol{\mathcal{H}}}^{\alpha,n}(\alpha=1,...,m). \tag{125a}$$

2. Compute algorithmic strain measures from current deformation gradient $\boldsymbol{F}^{n+1}$.

$$\begin{array}{rclcrcl} J^{n+1} &=& \det \boldsymbol{F}^{n+1} & & \bar{\boldsymbol{F}}^{n+1} &=& J^{n+1^{-1/3}}\boldsymbol{F}^{n+1} \\ \boldsymbol{C}^{n+1} &=& \boldsymbol{F}^{T,n+1}\boldsymbol{F}^{n+1} & & \bar{\boldsymbol{C}}^{n+1} &=& \bar{\boldsymbol{F}}^{T,n+1}\bar{\boldsymbol{F}}^{n+1} \end{array} \tag{125b}$$

3. Update stresses and electrical displacement:

$$\boldsymbol{S}^{n+1}=(\boldsymbol{S}^{\infty}_{vol}+\boldsymbol{S}^{\infty}_{iso}+\sum_{\alpha}\boldsymbol{Q}_{\alpha}+\boldsymbol{S}_{elem})|^{n+1}. \tag{125c}$$

with the following terms:

$$\begin{array}{rcl} \boldsymbol{S}^{\infty,n+1}_{vol} &=& \left(Jp\boldsymbol{C}^{-1}\right)|^{n+1} \\ \boldsymbol{S}^{\infty,n+1}_{iso} &=& \left(2J^{-2/3}\mathbb{P}:\sigma\boldsymbol{I}\right)|^{n+1} \\ \boldsymbol{Q}^{n+1}_{\alpha} &=& J^{n+1^{-2/3}}\mathbb{P}^{n+1}:\{\beta_{\alpha}exp[-\Delta t/2\tau_{\alpha}]J^{n+1^{2/3}}\bar{\boldsymbol{S}}^{\infty,n+1}_{iso}+\bar{\boldsymbol{\mathcal{H}}}^{\alpha,n}\} \\ \boldsymbol{S}^{n+1}_{elem} &=& \dfrac{\epsilon J}{2}[\boldsymbol{C}^{-1}:(\mathbb{E}\otimes\mathbb{E})]\boldsymbol{C}^{-1}-\epsilon J[\boldsymbol{C}^{-T}\mathbb{E}\otimes\boldsymbol{C}^{-T}\mathbb{E}]|^{n+1} \end{array} \tag{125d}$$

$$-\mathbb{D}^{n+1}=\left(-\epsilon J\boldsymbol{C}^{-T}\mathbb{E}\right)|^{n+1}. \tag{125e}$$

4. Compute current moduli:

5. Compute and save history variables:

$$\bar{\boldsymbol{\mathcal{H}}}^{\alpha,n+1}=exp[-\Delta t/\tau_{\alpha}]\bar{\boldsymbol{Q}}^{n+1}_{\alpha}-\beta_{\alpha}exp[-\Delta t/2\tau_{\alpha}]J^{n+1^{2/3}}\bar{\boldsymbol{S}}^{\infty,n+1}_{iso} \tag{125f}$$

5. Numerical Implementation of Finite Electromechanics

Since analytical solutions for the geometrically- and physically-nonlinear boundary value problems of finite electromechanics can be derived only for a limited number of special cases, computational methods must be employed in general. In this section a finite element model is proposed which allows the computation of approximate numerical solutions to the variational problem of finite strain electromechanics.

5.1. Electro-Mechanical Boundary Value Problem

The boundary value problem of a coupled electro-mechanical solid is outlined below. To formulate the variational principle we use compact notation which is introduced before. It is a coupled two field problem with displacement field $\boldsymbol{u}$ describing the mechanical response and the electric potential ϕ^e characterizing the electrical response.

$$\boldsymbol{u} : \begin{cases} \mathcal{B} \times [0,t] \to \mathbb{R}^3, \\ (\boldsymbol{x},t) \mapsto \boldsymbol{x} = \boldsymbol{\varphi}(\boldsymbol{X},t) \end{cases} \quad , \quad \phi^e : \begin{cases} \mathcal{B} \times [0,t] \to \mathbb{R}, \\ (\boldsymbol{x},t) \mapsto \phi^e(\boldsymbol{X},t) \end{cases} . \tag{126}$$

For a sophisticated illustration of the balance principles in terms of the primary fields we define a generalized deformation map $\mathfrak{U}$

$$\mathfrak{U} = [\boldsymbol{\varphi}(\boldsymbol{X},t), -\phi^e(\boldsymbol{X},t)]^T \tag{127}$$

As we consider the case of large strains, we need to have the Frechet derivative of the deformation map as the deformation gradient:

$$\boldsymbol{F} = \nabla_{\boldsymbol{X}} \boldsymbol{\varphi}(\boldsymbol{X},t) \tag{128}$$

In order to have the electric field to be curl free, based on the Maxwell's equation, it is defined as the gradient of the electric potential:

$$\mathbb{E} = -\nabla_{\boldsymbol{X}} \phi^e(\boldsymbol{x},t) \tag{129}$$

The above gradients describing the kinematics can be expressed by defining a generalized gradient $\boldsymbol{\mathcal{G}}$

$$\mathfrak{F} := \boldsymbol{\mathcal{G}}\left[\mathfrak{U}\right], \tag{130}$$

where $\mathfrak{F}$ is the generalized co-vector stated in section 2.5. The balance principles of coupled electro-mechanics are stated as

$$\mathrm{Div}\left[\boldsymbol{P}\right] + \rho\bar{\Gamma} = 0 \quad \text{and} \quad \mathrm{Div}\left[\mathbb{D}\right] - \bar{\rho}_0^e = 0 \tag{131}$$

where $\boldsymbol{P}$ is the first Piola Kichhoff stress, $\bar{\Gamma}$ is the body force, $\mathbb{D}$ is the electric displacement and $\bar{\rho}_0^e$ is the free volume charge density. Equations in (130) are expressed in a compact manner by using a generalized divergence operator $\mathscr{D}_v$ in terms of generalized vector.

$$\mathscr{D}_v\left[\mathfrak{S}\right] + \bar{\mathfrak{B}} = 0 \tag{132}$$

with $\bar{\mathfrak{B}}$ as the generalized body force vector

$$\bar{\mathfrak{B}} = \left[\rho\bar{\Gamma}, \bar{\rho}_0^e\right]^T \tag{133}$$

The generalized vector has been stated before shown to have the following relation with the generalized covector through the mixed energy enthalpy potentioal funtion $\Psi(\mathfrak{F})$.

$$\mathfrak{S} = \partial_{\mathfrak{F}} \Psi(\mathfrak{F}; \boldsymbol{X}) \tag{134}$$

The boundary conditions are stated distinctly for the case of mechanical and electrical problem as:

$$\boldsymbol{\varphi} = \bar{\boldsymbol{\varphi}}(\boldsymbol{X}, t) \quad \text{on} \quad \partial\mathcal{B}_{\boldsymbol{\varphi}} \quad \text{and} \quad \boldsymbol{P}\boldsymbol{N} = \bar{\boldsymbol{T}}(\boldsymbol{X}, t) \quad \text{on} \quad \partial\mathcal{B}_T, \tag{135}$$

and

$$\phi^e = \bar{\phi}^e(\boldsymbol{x}, t) \quad \text{on} \quad \partial\mathcal{B}_{\phi^e} \quad \text{and} \quad [\![\mathbb{D}]\!] \cdot \boldsymbol{N} = \bar{\Sigma}^e(\boldsymbol{x}, t) \quad \text{on} \quad \partial\mathcal{B}_\Sigma. \tag{136}$$

Using a sophisticated mode of presentation one could rewrite the above boundary conditions as

$$\mathfrak{U} = \bar{\mathfrak{U}}(\boldsymbol{X}, t) \quad \text{on} \quad \partial\mathcal{B}_{\mathfrak{U}} \quad \text{and} \quad \mathfrak{S} \star \mathfrak{N} = \bar{\mathfrak{T}}(\boldsymbol{X}, t) \quad \text{on} \quad \partial\mathcal{B}_{\mathfrak{T}} \tag{137}$$

where the generalized vector $\bar{\mathfrak{U}} = \left[\bar{\boldsymbol{\varphi}}, \bar{\phi}^e\right]$ prescribes the values on its corresponding boundary $\partial\mathcal{B}_{\mathfrak{U}} = [\partial\mathcal{B}_{\boldsymbol{\varphi}}, \partial\mathcal{B}_{\phi^e}]$. Analogously, we apply the so called generalized traction vector $\bar{\mathfrak{T}} = \left[\bar{T}, \bar{\Sigma}^e\right]$ on its respective boundary $\partial\mathcal{B}_{\mathfrak{T}} = [\partial\mathcal{B}_T, \partial\mathcal{B}_\Sigma]$.

5.2. Continuus Variational Formulation

Let us assume the existence of an incremental energy functional $I(\mathfrak{U})$ for both generalized vectors and loads. This assumption is common in many fields of solid mechanics. Furthermore, we assume that the loads do not depend on the motion of the body. It means that the directions of the loads remain parallel and their values unchanged throughout the deformation process. The total generalized incremental energy functional $I(\mathfrak{U})$ of the system is defined as the difference between the internal energy stored in the body and the total work done by the external loads in the time interval $[t_n, t_{n+1}]$.

$$I(\mathfrak{U}) = I_{int}(\mathfrak{U}) - I_{ext}(\mathfrak{U}) \tag{138}$$

with

$$\begin{aligned} I_{int}(\mathfrak{U}) &= \int_{\mathcal{B}} \Psi(\boldsymbol{\mathcal{G}}[\mathfrak{U}]; \boldsymbol{X}) dV \\ I_{ext}(\mathfrak{U}) &= \int_{\mathcal{B}} \bar{\mathfrak{B}} \star (\hat{\mathfrak{U}} - \hat{\mathfrak{U}}_n) dV + \int_{\partial\mathcal{B}_{\mathfrak{T}}} \bar{\mathfrak{T}} \star (\hat{\mathfrak{U}} - \hat{\mathfrak{U}}_n) dA. \end{aligned} \tag{139}$$

in terms of the generalized generalized quantities introduced in section 2.5. Here in 139 $\hat{\mathfrak{U}}$ is defined as $\mathfrak{U} - [\boldsymbol{X}, 0]^T$. We use the minimization principle to obtain the generalized displacement fields, satisfying the Dirichlet boundary conditions, corresponding to the state of equilibrium.

$$\mathfrak{U} = \text{Arg}\left\{\text{stat}_{\mathfrak{U}\in\mathcal{W}} I(\mathfrak{U})\right\} = \text{Arg}\left\{\inf_{\boldsymbol{\varphi}} \sup_{-\phi^e} I(\boldsymbol{\varphi}, -\phi^e)\right\} \tag{140}$$

with

$$\mathfrak{U} \in \mathcal{W} := \{\mathfrak{U} | \mathfrak{U}(\boldsymbol{X}, t) \quad \text{on} \quad \partial\mathcal{B}_{\mathfrak{U}}\} \tag{141}$$

As we see above the functional $I(\mathfrak{U})$ is to be maximized subject to the electric potential and minimized with respect to the displacement field leading to a saddle point structure. The variational of the functional gives the necessary condition

$$\delta I(\mathfrak{U}, \delta\mathfrak{U}) = \left[\frac{d}{d\epsilon} I(\mathfrak{U} + \epsilon\delta\mathfrak{U})\right]_{\epsilon=0} = 0. \tag{142}$$

In this way the problem is reduced to an ordinary minimum problem of differential calculus with respect to the single variable ϵ. The minimum is obtained for $\epsilon = 0$. The arbitrary generalized displacement vector satisfies the homogeneous boundary conditions i.e. $\delta\mathfrak{U} = \boldsymbol{0}$ on $\partial\mathcal{B}_{\mathfrak{U}}$ where the generalized displacement takes the prescribed value. With the above requirements we get the variational resulting in the Euler-Lagrange equations which implicitly satisfy the Neumann boundary conditions

$$\delta I(\mathfrak{U}, \delta\mathfrak{U}) = \int_{\mathcal{B}} \left\{\partial_{\mathfrak{F}}\Psi \star \boldsymbol{\mathcal{G}}[\delta\mathfrak{U}] - \bar{\mathfrak{B}} \star \delta\mathfrak{U}\right\} dv - \int_{\partial\mathcal{B}_T} \bar{\mathfrak{T}} \star \delta\mathfrak{U}\, dA = 0. \tag{143}$$

5.3. Finite Element Discretization

In the standard finite element approach the *spatial discretization* of the continuum body $\mathcal{B}$ is based on its approximate subdivision into a set of N finite elements $\mathcal{B}^e \subset \mathcal{B}^h$, such that

$$\mathcal{B} \approx \mathcal{B}^h = \bigwedge_{e=1}^{N} \mathcal{B}^e \ , \tag{144}$$

where the symbol $\bigwedge_{e=1}^{N}$ denotes the standard finite element assembly operator. One further defines a reference element $\mathcal{A}^e$ with local coordinates $\boldsymbol{\theta}$, as shown in Figure 11. The variational problem (143) is approximately solved by a finite element method. To this end, the generalized deformation map and its gradient are discretized within N finite element domains $\mathcal{B}^e \subset \mathcal{B}^h$ in which the discretized solid $\mathcal{B}^h$ is decomposed, such that:

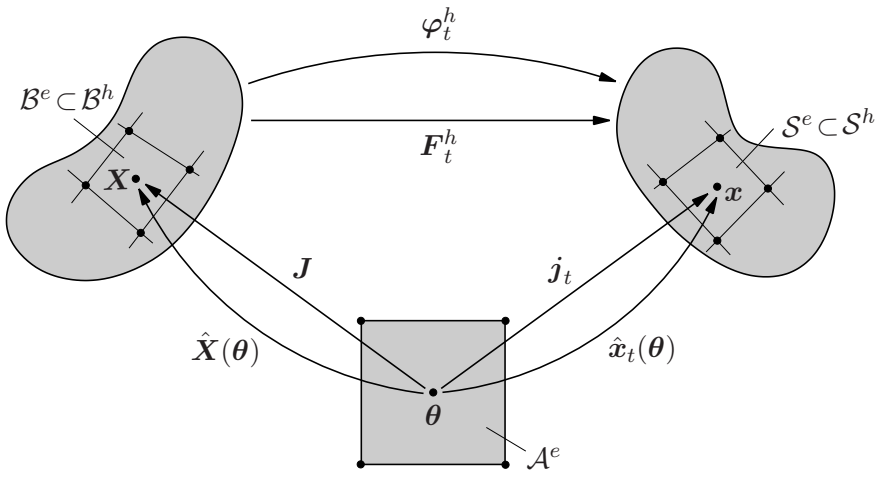

Figure 11: Isoparametric mappings between the element parameter space $\mathcal{A}^e$ and the associated finite elements $\mathcal{B}^e \subset \mathcal{B}^h$ and $\mathcal{S}^e \subset \mathcal{S}^h$ in the Lagrangian and Eulerian settings.

The coordinates of the element in the material setting $\boldsymbol{X}^h \in \mathcal{B}^e$ and the spatial setting $\boldsymbol{x}^h \in \mathcal{S}^e$ are then described by the isoparametric *Lagrangian* and *Eulerian parameter maps*

$$\hat{\boldsymbol{X}} := \begin{cases} \mathcal{A}^e \to \mathcal{B}^e \subset \mathcal{B}^h \ , \\ \boldsymbol{\theta} \mapsto \boldsymbol{X}^h = \hat{\boldsymbol{X}}(\boldsymbol{\theta}) \end{cases} , \qquad \hat{\boldsymbol{x}}_t := \begin{cases} \mathcal{A}^e \to \mathcal{S}^e \subset \mathcal{S}^h \ , \\ \boldsymbol{\theta} \mapsto \boldsymbol{x}^h = \hat{\boldsymbol{x}}_t(\boldsymbol{\theta}) \end{cases} . \tag{145}$$

These mappings approximate the material and spatial coordinates on the basis of the standard expressions

$$\boldsymbol{X} \approx \boldsymbol{X}^h = \hat{\boldsymbol{X}}(\boldsymbol{\theta}) = \sum_{\alpha=1}^{n_{npe}} \hat{N}^\alpha(\boldsymbol{\theta}) \boldsymbol{D}^\alpha = \hat{\boldsymbol{N}}(\boldsymbol{\theta}) \boldsymbol{D} \ , \tag{146a}$$

$$\boldsymbol{x} \approx \boldsymbol{x}^h = \hat{\boldsymbol{x}}_t(\boldsymbol{\theta}) = \sum_{\alpha=1}^{n_{npe}} \hat{N}^\alpha(\boldsymbol{\theta}) \boldsymbol{d}_t^\alpha = \hat{\boldsymbol{N}}(\boldsymbol{\theta}) \boldsymbol{d}_t \ , \tag{146b}$$

where n_{npe}, denotes the number of nodes per element, $\hat{\boldsymbol{N}}$ represents the matrix of shape functions parameterized in the local coordinates $\boldsymbol{\theta} \in \mathcal{A}^e$ of the finite element parameter space. The vectors $\boldsymbol{D} \in \mathbb{R}^{\dim \cdot n_{npe}}$ and $\boldsymbol{d}_t \in \mathbb{R}^{\dim \cdot n_{npe}}$, where $\dim \in \{1,2,3\}$ are the spatial dimensions of the considered problem, contain the discrete Lagrangian and Eulerian nodal positions of element $\mathcal{B}^e$ at time t, respectively. Based on the introduced approximate mappings and again referring to Figure 11, the deformation map can be expressed as

$$\boldsymbol{\varphi}_t^h(\boldsymbol{X}^h) := \hat{\boldsymbol{x}}_t \circ \hat{\boldsymbol{X}}^{-1} = \hat{\boldsymbol{x}}_t\big(\boldsymbol{\theta}(\boldsymbol{X}^h)\big) \ . \tag{147}$$

One may further define the gradients

$$\boldsymbol{J} := \partial_{\boldsymbol{\theta}} \hat{\boldsymbol{X}} = \partial_{\boldsymbol{\theta}} \Big[\sum_{\alpha=1}^{n_{npe}} \hat{N}^\alpha(\boldsymbol{\theta}) \boldsymbol{D}^\alpha \Big] = \sum_{\alpha=1}^{n_{npe}} \boldsymbol{D}^\alpha \otimes \partial_{\boldsymbol{\theta}} \hat{N}^\alpha(\boldsymbol{\theta}), \text{ with } J^A{}_i = \frac{\partial \hat{X}^A}{\partial \theta^i} = \sum_{\alpha=1}^{n_{npe}} \hat{N}^\alpha_{,i} (\boldsymbol{D}^\alpha)^A,$$

$$\boldsymbol{j}_t := \partial_{\boldsymbol{\theta}} \hat{\boldsymbol{x}} = \partial_{\boldsymbol{\theta}} \Big[\sum_{\alpha=1}^{n_{npe}} \hat{N}^\alpha(\boldsymbol{\theta}) \boldsymbol{d}_t^\alpha \Big] = \sum_{\alpha=1}^{n_{npe}} \boldsymbol{d}_t^\alpha \otimes \partial_{\boldsymbol{\theta}} \hat{N}^\alpha(\boldsymbol{\theta}), \text{ with } j^a{}_i = \frac{\partial \hat{x}^a}{\partial \theta^i} = \sum_{\alpha=1}^{n_{npe}} \hat{N}^\alpha_{,i} (\boldsymbol{d}_t^\alpha)^a.$$

Note that, based on the chain rule, the above mappings may be utilized to related derivatives in parameter space to derivatives in the reference and current configurations via

$$\operatorname{Grad} \hat{\boldsymbol{N}} = \boldsymbol{J}^{-T} \partial_{\boldsymbol{\theta}} \hat{\boldsymbol{N}} \ , \qquad \operatorname{grad} \hat{\boldsymbol{N}} = \boldsymbol{j}_t^{-T} \partial_{\boldsymbol{\theta}} \hat{\boldsymbol{N}} \ . \tag{148}$$

With these definitions at hand, the deformation gradient is approximated as

$$\boldsymbol{F}_t^h = \operatorname{Grad} \boldsymbol{\varphi}_t^h(\boldsymbol{X}^h) = \operatorname{Grad} \big[\hat{x}_t\big(\boldsymbol{\theta}(\boldsymbol{X}^h)\big) \big] = \partial_{\boldsymbol{\theta}} \hat{x}_t \, \partial_{\boldsymbol{X}^h} \boldsymbol{\theta} = \boldsymbol{j}_t \boldsymbol{J}^{-1} =: \hat{\boldsymbol{B}} \boldsymbol{d}_t \ . \tag{149}$$

The matrix $\hat{\boldsymbol{B}}(\boldsymbol{X}^h)$ contains the derivatives of the shape functions with respect to the Lagrangian coordinates $\boldsymbol{X}^h$.[3] Following the *isoparametric concept*, in which the geometry

[3]The compact notation matrix relation $\boldsymbol{F}_t^h = \hat{\boldsymbol{B}} \boldsymbol{d}_t$ is to be interpreted in the sense that

$$F^a{}_A = \sum_{\alpha=1}^{n_{npe}} \frac{\partial \hat{N}^\alpha}{\partial \theta^i} (\boldsymbol{d}_t^\alpha)^a (\boldsymbol{J}^{-1})^i{}_A = \sum_{\alpha=1}^{n_{npe}} (\boldsymbol{d}_t^\alpha)^a \frac{\partial \hat{N}^\alpha}{\partial \boldsymbol{X}^A} = \sum_{\alpha=1}^{n_{npe}} (\boldsymbol{d}_t^\alpha)^a \hat{B}^\alpha{}_A \ . \tag{150}$$

and the field variables are approximated over the element domain by the same set of shape functions.

Utilizing again the compact notation concept that was used for the concise representation of the variational problem, we introduce the *element generalized displacement vector* $\mathfrak{D}'^e$, which contains the element nodal displacements $\boldsymbol{d}^e$ and the negative electric nodal potential $-\phi^e$ at the current time t_{n+1}.

$$\mathfrak{D}'^e = [\boldsymbol{d}^e, -\phi^e] \tag{151}$$

After assembling the element quantities in global arrays:

$$\mathfrak{D}' = \bigwedge_{e=1}^{N} \mathfrak{D}'^e \quad , \quad \mathfrak{N}'(\boldsymbol{X}) = \bigwedge_{e=1}^{N} \mathfrak{N}'^e(\boldsymbol{X}) \quad , \quad \mathfrak{B}'(\boldsymbol{X}) = \bigwedge_{e=1}^{N} \mathfrak{B}'^e(\boldsymbol{X}) \tag{152}$$

Note that we have dropped the superscript t. It is henceforth implied that all discrete variables are evaluated at the current time t, or more accurately at the discrete time t_{n+1} at the end of the current time interval. The *discrete generalized primary variable vector* and *discrete generalized deformation gradient* are then computed from the relations

$$\mathfrak{U}'^h = \mathfrak{X}' + \mathfrak{N}'(\boldsymbol{X})\mathfrak{D}' \quad , \quad \mathcal{G}[\mathfrak{U}'^h] = \mathfrak{I}' + \mathfrak{B}'(\boldsymbol{X})\mathfrak{D}' \tag{153}$$

where the arrays $\mathfrak{X}'$ and $\mathfrak{I}'$ are defined as:

$$\mathfrak{X}' = \begin{bmatrix} \boldsymbol{X} \\ \boldsymbol{0} \end{bmatrix} \quad \text{and} \quad \mathfrak{I}' = \begin{bmatrix} \boldsymbol{1} & \boldsymbol{0} \\ \boldsymbol{0} & \boldsymbol{0} \end{bmatrix} \tag{154}$$

Using above approximation in the continous form of the energy functional (138) will give us the approximated form of the energy functional as follows:

$$I'^h(\mathfrak{D}') = \int_{\mathcal{B}^h} \Psi(\mathfrak{I}' + \mathfrak{B}'\mathfrak{D}') - \bar{\mathfrak{B}}' \star \mathfrak{N}'\Delta\mathfrak{D}'dV - \int_{\mathcal{B}^h_{\bar{\mathfrak{T}}'}} \bar{\mathfrak{T}}' \star \mathfrak{N}'\Delta\mathfrak{D}'dA \tag{155}$$

with $\Delta\mathfrak{D}' := \mathfrak{D}' - \mathfrak{D}'_n$. The discrete energy functional has to be stationary with respect to the global generalized nodal displacement $\mathfrak{D}'$. The necessary condition for this can be obtained by setting the variation of $I'^h(\mathfrak{D}')$ to zero.

$$\delta I'^h(\mathfrak{D}') = I'^h_{,\mathfrak{D}'}(\mathfrak{D}') = 0 \tag{156}$$

By defining the analogous approximations $\delta\mathfrak{U}^h = \mathfrak{N}\,\delta\mathfrak{D}$ and substituting into (156), one obtains the discrete equivalent of the necessary condition for stationarity in the continuous setting as

$$\delta I'^h = \int_{\mathcal{B}_h} \mathfrak{B}'^T \mathfrak{S}'^h - \mathfrak{N}'^T \bar{\mathfrak{B}}' dV - \int_{\partial\mathcal{B}'_{\bar{\mathfrak{T}}'}} \mathfrak{N}^T \bar{\mathfrak{T}} dA = 0 \tag{157}$$

where the *finite element residual vector* can been defined as $\mathfrak{R}' := \delta I'^h(\mathfrak{D}')$. Equation (157) represents a nonlinear algebraic system for the determination of the generalized displacement vector $\mathfrak{D}'$ of the coupled electro-mechanical problem. To find the roots of the nonlinear problem $\mathfrak{R}' = \boldsymbol{0}$, an iterative solution procedure must be employed.

Following a standard *Newton-Raphson scheme*, one obtains the following update relation for the nodal degree of freedom vector

$$\mathfrak{D}' \Leftarrow \mathfrak{D}' - \left[I'^{h}_{,\mathfrak{D}'\mathfrak{D}'}(\mathfrak{D}')\right]^{-1} I'^{h}_{,\mathfrak{D}'}(\mathfrak{D}') \tag{158}$$

The iteration procedure is terminated if the norm of the residual falls below as certain tolerance, i.e. $\|\mathfrak{R}'\| < tol$. In the preceding expressions we have utilized the definitions of the *finite element tangent matrix*

$$\mathfrak{K}' := I'^{h}_{,\mathfrak{D}'\mathfrak{D}'}(\mathfrak{D}') = \int_{\mathcal{B}^h} \mathfrak{B}'^{T} \mathfrak{C}'^{h} \mathfrak{B}' \, dV \tag{159}$$

where we have assumed dead loads, and the *discrete generalized stresses* and *discrete coupled moduli*

$$\mathfrak{S}'^{h} := \partial_{\mathfrak{F}'^{h}} \Psi \quad , \quad \mathfrak{C}'^{h} := \partial^2_{\mathfrak{F}'^{h}\mathfrak{F}'^{h}} \Psi \tag{160}$$

It must be emphasized that due to the chosen variational formulation the tangent matrix $\mathfrak{K}'$ is automatically *symmetric*, and consequently solvers for symmetric linear systems of equations can be employed in the iterative solution procedure of the nonlinear problem.

6. Numerical Results

6.1. Basic Tests

To test the proposed models, we would like to see the response to some simple deformation and force driven tests at the *material point level*. To achieve this, we present below, some *basic numerical experiments* which are essential to show the desired viscoelastic behaviour of the material to some simple deformation processes. The results of these tests should help us show the behaviour of the material and analyse the results of boundary value problems presented later in this chapter.

6.1.1. Relaxation Test. Stress relaxation describes how material relieve stress under constant strain. Because of viscoelasticity, material behaves in a nonlinear fashion. This nonlinearity can be described by both stress relaxation and a creep tests. In the relaxation test a stepwise strain is imposed with raising time of t_1 and the stress is monitored. Moreover, It is of interest to see how the response of the model to stepwise one dimensional deformation is altered by the electric field. To observe this we need to apply a one dimensional deformation at different electric fields and look at the stress response. So we apply in parallel an electric field with the same raising time of $t_1^\phi = t_1 = 0.5$ *sec.* Maximum amount of engineering strain is chosen to be $\varepsilon_{11} = \%10$. Results have been taken at gauss point in the midle of the plain in order to show the material response at gauss point level.

As shown before, Arrunda-Boyce material[1], is used for elastic material model in this work. Set of material parameters of electro viscoelastic model which have been used here are show in Table(1). The elastic and viscoelastic parameters have been used before by Ask et. al. [2], and the electric permitivity has been set experimentally by Ask et. al. [25].

Table 1: Material parameters for *viscoelastic electroactive polymer* based on *isotropic Arrunda-Boyce elastomer model.*

Elastic Material Properties:		
$\kappa = 3.2 \times 10^3\,\mathrm{N/mm^2}$	$\mu = 1.8\,\mathrm{N/mm^2}$	$N = 2.7$
Viscoelastic Material Properties:		
$\beta = 1.0$	$\tau_d = 0.4\,\mathrm{sec}$	
Electrical Material Properties:		
$\epsilon = 41.6 \times 10^{-6}\,\mathrm{N/mm^2}$		

Using above parameters, we plot first Piola stress vs. time for different electric fields as shown in Figure 12. Exponentially decaying stress which is characteristic behavior of relaxation tests is reproduced in the results. Electric field tends to shrink the specimen, therefore the stress will be increased with increasing electric field. The test is done with different electric fields and this effect can be traced there. As depicted in Figure 12, relaxation behavior can be seen in all tests and stress is higher for higher electrical fiels.

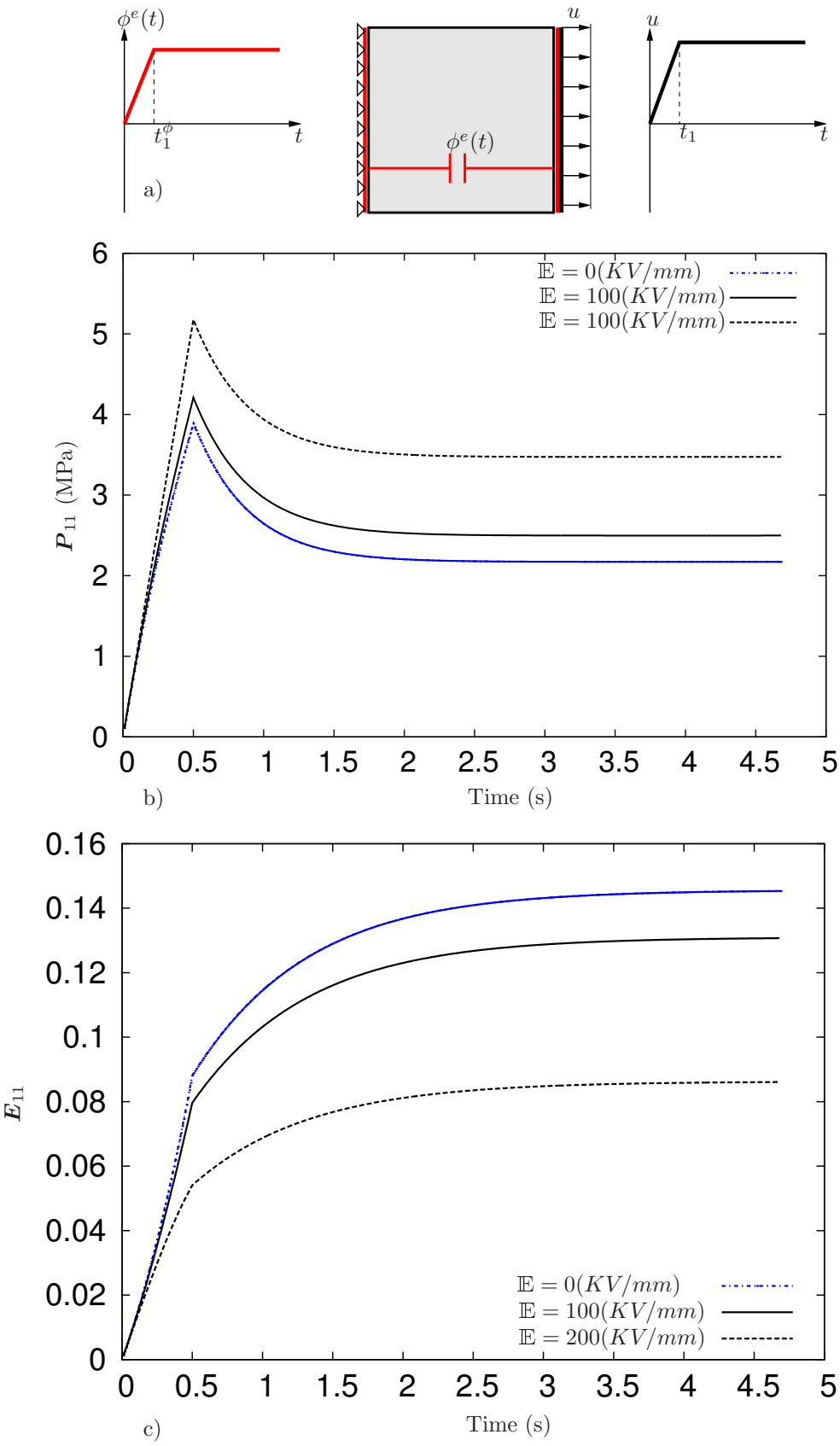

Figure 12: a)Test schematic for obtaining viscoelastic material behaviour of the model , b)Relaxation test behaviour of material model at Gauss point level , c)Creep test behaviour of material model at Gauss point level (It is obtained by replacing force boundary condition instead of displacement in schematic view of the test)

6.1.2. Creep Test. When a viscoelastic material is subjected to a constant load, it deforms continuously. The initial strain is roughly predicted by its stress-strain modulus. The material will continue to deform slowly with time until reaching a certain point. In the early stage of loading the creep rate decreases rapidly with time. Then it reaches a fairly steady state stage. This phenomenon of deformation under load with time is called creep.

To track the creep behaviour of the material, a stepwise one dimensional force is applied on the specimen. Furtheremore to observe the effect of electric field we need to apply a one dimensional force at different electric fields and look at the strain response. So we apply in parallel an electric field with the same raising time of $t_1^{\phi} = t_1 = 0.5$ *sec.*

Results are shown using plot of Cauchy strain vs. time for different electric fields in Figure 12. The effect of electric field, which is depicted in Figure 12, shows decreas of strain due to force. This can be interpreted, having in mind shrinking effect of electric field in Dielectric Elastomers. As it can be seen from the above results viscoelastic behavior is modeled successfully at large strains in presence of electric field. To further show the capability of the model we will test it for cyclic loading in the next section.

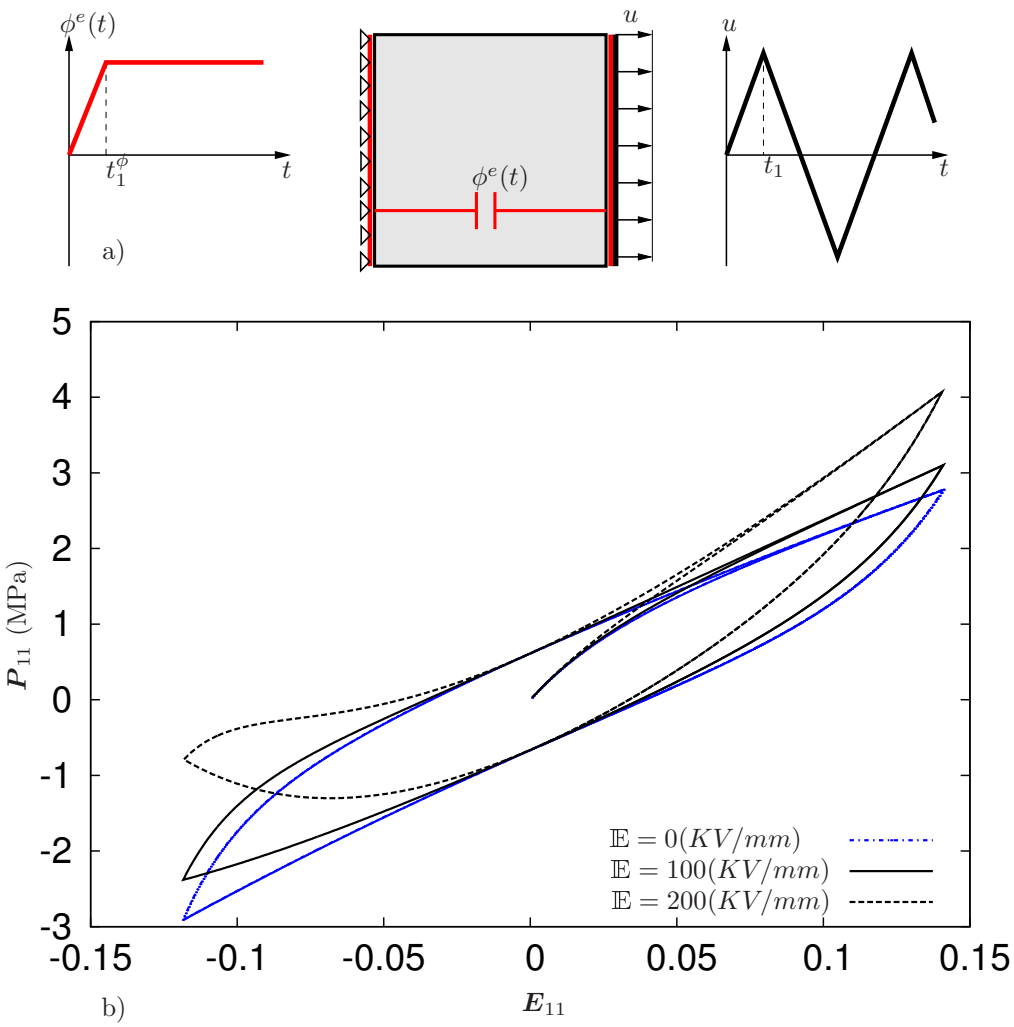

Figure 13: a)Test schematic of behaviour of material model at Gauss point level for cyclic loading, b)Cyclic test behaviour of material model at Gauss point level

6.1.3. Cyclic Loading. Cyclic loading leads to hysteresis (a phase lag) and thus a dissipation of mechanical energy in viscoelastic materials. The final test at gauss point level which is conducted here is cyclic loading. To perform this test we use the same sample as previous tests and impose a cyclic displacement as depicted in Figure 13.a. Characteristic time of the loading is equal to the previous cases and thus time period of one cycle will be $T = 4 \times t_1 = 2\,sec$. Hysteresis curves are shown in Figure 13.b. Shrinking effect of electric field plays an evident role here. This will increase amount of stress in the tension phase and decreases it in the compression phase.

6.2. Selected Boundary Value Problems

In this project we have implemented 2D-Quad plain strain and 3D-Hex (Brick) elements as well as viscoelastic electromechanical material model within FEAP finite element code. In order to show the reliability and capability of our code, we shall show some two and three dimensional model problems which have been solved by it in this section.

6.2.1. Non Homogeneous Response Test in 2D. Testing the code in a non homogeneous example motivates us to consider a boundary value problem of the type shown in Figure 14. Here, we have a hard metal inclusion with a different material properties in the same polymeric matrix. Inclusion has different material properties. Bulk modulus is $\kappa = 100 \times 10^6\,\mathrm{N/mm^2}$, shear modulus $\mu = 50 \times 10^6\,\mathrm{N/mm^2}$ and electric permitivity $\epsilon = 4.6 \times 10^{-6}\,\mathrm{N/mm^2}$. Other properties are identical to Table (1).

Loading procedure is as follows. Electric potential on the upper and lower edges of the speciemen is specifies and track a ramp untill $t_1^\phi = 2\,\mathrm{sec}$. After this stage the potential is set to be constant. Final shape of the specimen with electric potential contours is displayed in Figure 15.

Figure 15 shows highly inhomogeneous response in both electrical potential and displacement fields. This is a result of different electric permitivity and elastic properties of inclusion. In order to show the viscoelastic effect a characteristic length of d is chosen to be plotted. This length is shown in Figure 14 and depicted in Figure 16 in order to show the nonlinear large strain and viscoelastic behavior of the material.

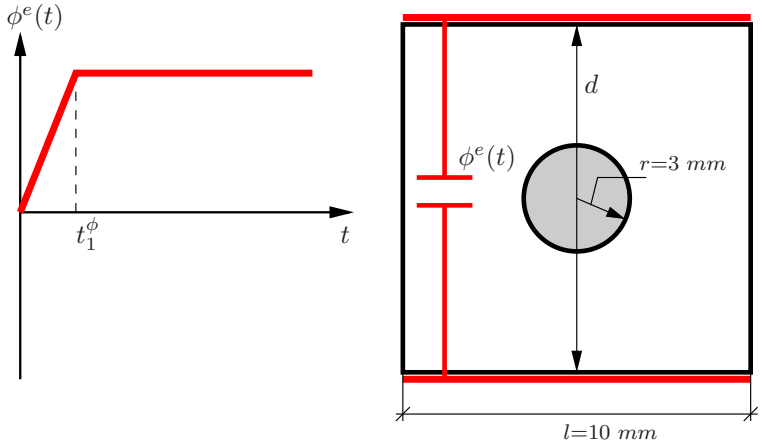

Figure 14: A polymeric specimen with an inclusion exposed to an electric field. This BVP will activate different modes of deformation due to inhomogeneity in the specimen and thus it is an appropriate bench problem to show the reliability of the code.

Due to the electrical loading it is first showing a nonlinear elastic response and after $t_1^{\phi} = 2\,\text{sec}$ as we maintain the electrical field it behaves like a material under creep. This example shows a viscoelastoc behaviour just under electrical loading.

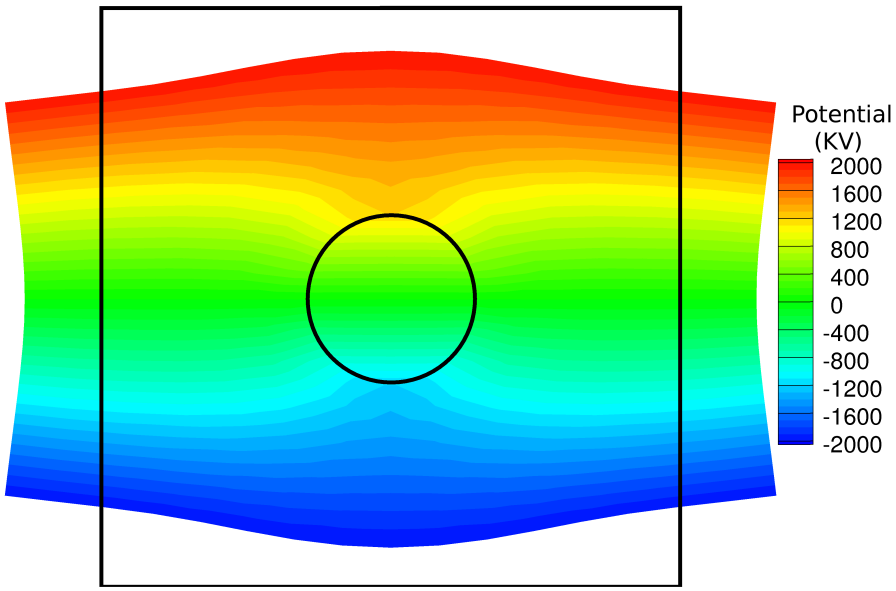

Figure 15: Electric potential contours in a deformed specimen. In order to show the amount of deformation, initial shape have been shown with solid lines.

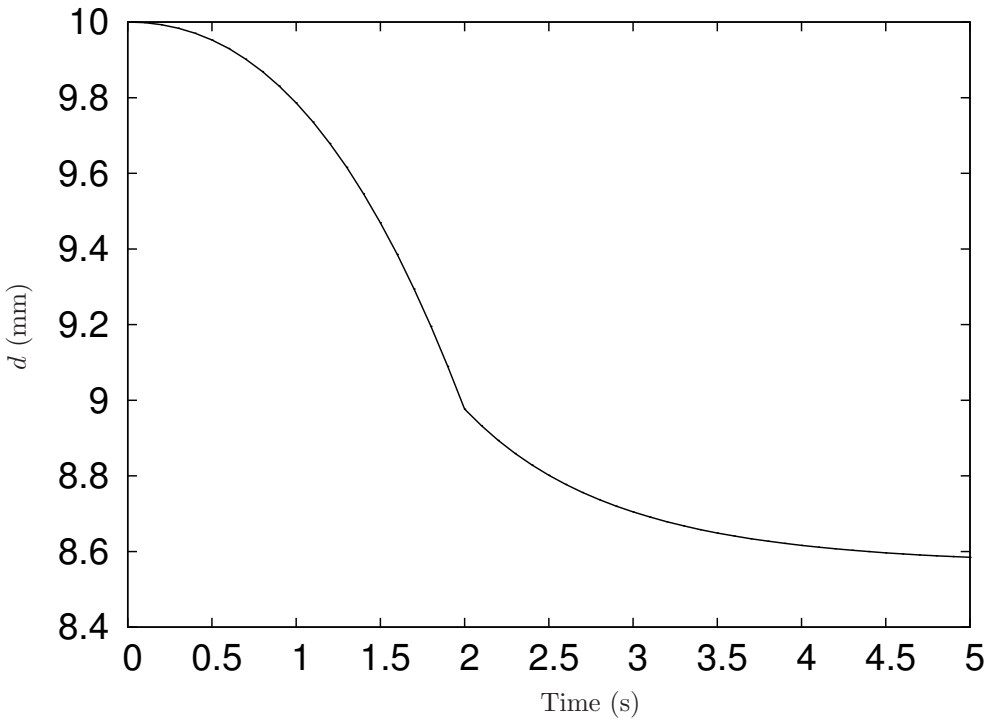

Figure 16: Characteristic width of the polymeric specimen with metallic inclusion under electrical loading. Keeping constant electric field after $t_1^{\phi} = 2$ (sec) leads to a creep like behavior. This behaviour is stimulated with only electrical field loading

6.2.2. Bi-Material (Finger) Actuator. One of the applications of electroactive materials is in the field of robotics. Since these materials deform on the application of electric field, they may be used in making finger actuators. Typically deformations in such applications are large and this is an area where finite strain modeling is required. In the example that follows, we model a finger as a composite bar in three dimensions using 3D Brick element and show how the bar deforms under application of electic fields. The example shows that finite strain modeling is indeed a requirement from a practical perspective. Figure 17 shows the boundary value problem definition of Finer actuator.

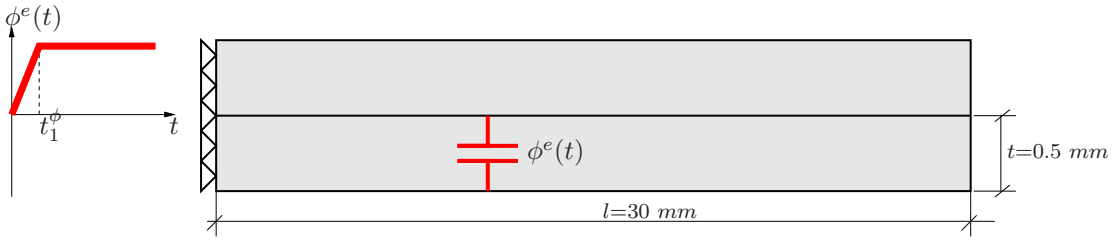

Figure 17: Definition of the boundary value problem. A stepwise electric potential difference $\phi^e(t)$ is applied between the midle and lower planes of the composite bar and the displacements at the left end are fixed. Thickness is considered to be z=4 mm.

In Figure 18 the undeformed mesh as well as deformed configuration has been shown without scaling the deformation. Quite large strains and deformations occurred in the beam. The lower layer thickness has been changed due to the applied electric field and the area of the lower one increase. This ends up to the bending of the entire structure. To obtain this deformation an electric field of 300KV/mm is applied. This is a relatively big electric voltage to be aplied experimentally. However, to show the capability of the model we applied this field in our numerical experiment.

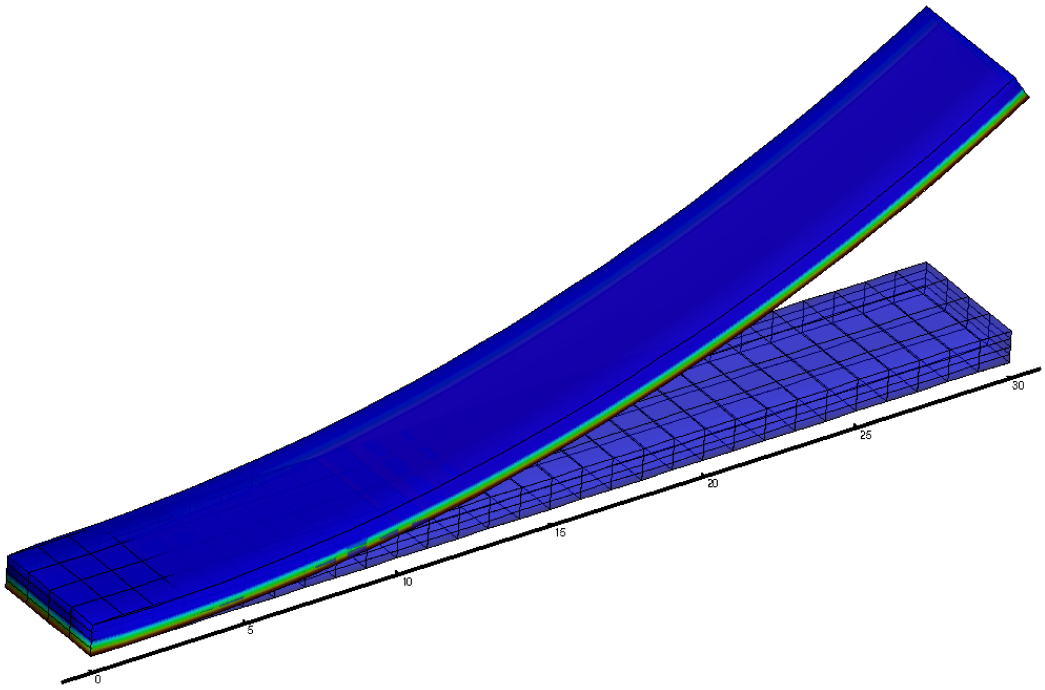

Figure 18: Deformed and undeformed configurations of the composite bar at applied potential differences ϕ^e = 300 KV/mm.

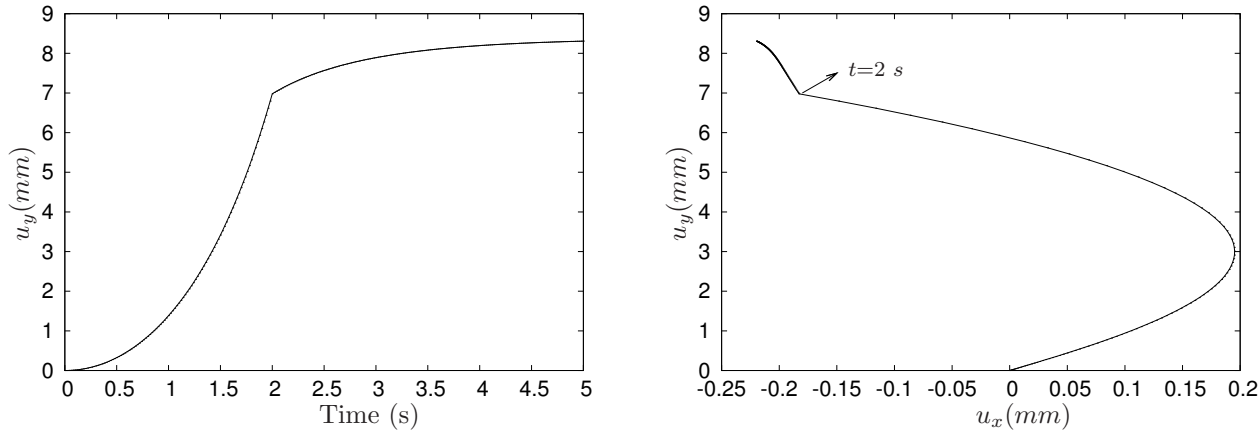

Figure 19: Beam tip deformation; vertical deformation versus time is shown in the left image which shows a creep behavior. Planar deformation image is shown in the right figure.

Figure 19 depicts beam tip deformation. The vertical deformation versus time shows a creep type behavior for the beam tip deformation when it is under constant electrical loading. The planar image of beam tip deformation reveals that first the lower layer tends to extend in x direction after that bending will happen. After $t = 2$s which is shown in the plot the nonlinear elastic part will be finished and the remaining beam tip movement is due to creep.

6.2.3. Double S-Shape Actuator. The deformation of the polymer film can be used in many different ways to produce actuation. Another possible configuration is the bimorph double-S-shaped-actuator. Here, two sheets of electroded polymer films are glued together and form a double-S-shape. If the external layers are active, the curvature of the actuator can be accentuated (see Figure 20) and otherwise diminished if the internal layers are active.

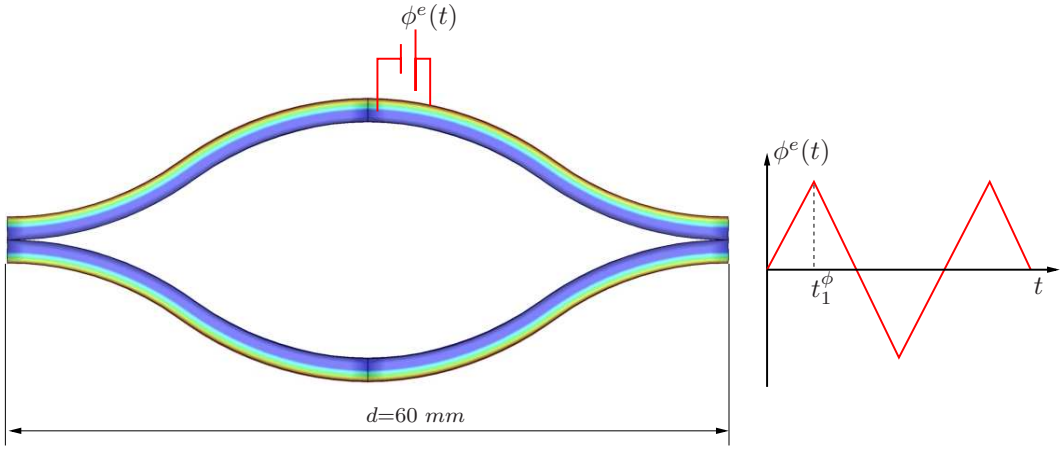

Figure 20: Hysteresis behavior of dielectric elastomer double S-shape actuator

In the case of viscoelasticity a hysteresis loop have been reported in several dielectric elastomer actuators(see e.g. Plante & Dubowsky [20]). In Figure 21 hysteresis curve of this actuator for the depicted loading is shown. To show the hysterisis we chose length of the actuatore as the charachteristic length and plted this length versus electrical field

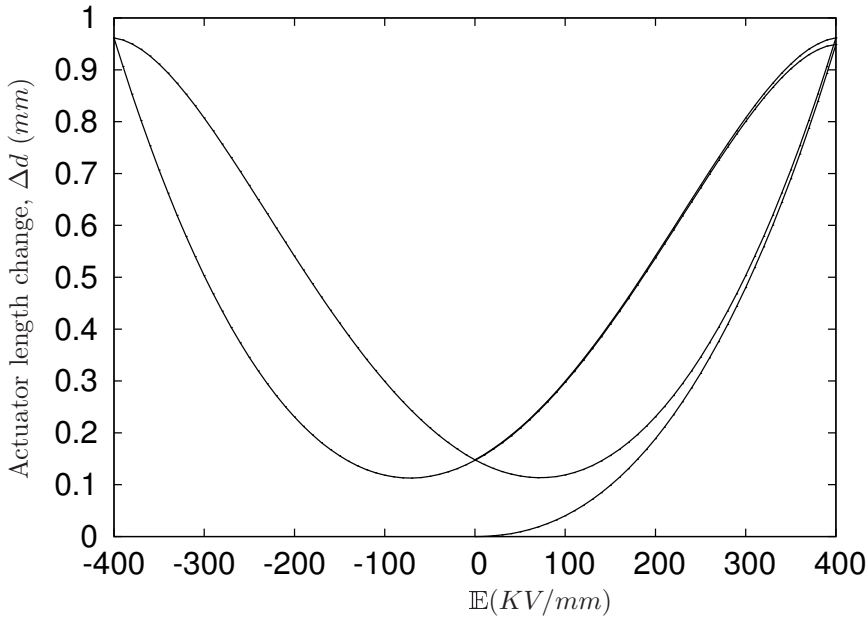

Figure 21: Hysteresis behavior of dielectric elastomer double S-shape actuator

which plays the role of force here.

References

[1] Arruda, E.M.; Boyce, M. [1993]: *A three-dimensional constitutive model for the large stretch behavior of rubber elastic materials.* Journal of the Mechanics and Physics of Solids, 41(2): 389–412.

[2] Ask, A.; Menzel, A.; Ristinmaa, M. [2010]: *On the modelling of electro-viscoelastic response of electrostrictive polyurethane elastomers.* In *IOP Conference Series: Materials Science and Engineering*, Vol. 10, page 012101. IOP Publishing.

[3] Brochu, P.; Pei, Q. [2010]: *Advances in dielectric elastomers for actuators and artificial muscles.* Macromolecular Rapid Communications, 31(1): 10–36.

[4] Coleman, B. D.; Noll, W. [1963]: *The Thermodynamics of Elastic Materials with Heat Conduction and Viscosity.* Archive for Rational Mechanics and Analysis, 13: 167–178.

[5] Eringen, A. C.; Maugin, G. A. [1990]: *Electrodynamics of Continua I — Foundations and Solid Media.* Springer-Verlag, New York.

[6] Govindjee, S.; Simo, J. [1992]: *Mullins effect and the strain amplitude dependence of the storage modulus.* International journal of solids and structures, 29(14-15): 1737–1751.

[7] Gurtin, M. E. [1981]: *An Introduction to Continuum Mechanics*, Vol. 158. Academic Press, San Diego.

[8] Holzapfel, G.A. [1996]: *On large strain viscoelasticity: continuum formulation and finite element applications to elastomeric structures.* International Journal for Numerical Methods in Engineering, 39(22): 3903–3926.

[9] Hughes, T.J.R.; Pister, K. [1978]: *Consistent linearization in mechanics of solids and structures.* Computers & Structures, 8(3-4): 391–397.

[10] Hutter, K.; Ven, A. A. F. van de [1978]: *Field Matter Interactions in Thermoelastic Solids*, Vol. 88 of *Lecture Notes in Physics.* Springer-Verlag, New York.

[11] Kaliske, M.; Rothert, H. [1997]: *On the finite element implementation of rubber-like materials at finite strains.* Engineering Computations, 14(2): 216–232.

[12] Lubliner, J. [1985]: *A model of rubber viscoelasticity.* Mechanics research communications, 12(2): 93–99.

[13] Marsden, J. E.; Hughes, T. J. R. [1983]: *Mathematical Foundations of Elasticity.* Prentice Hall, Englewood Cliffs, NJ.

[14] Maugin, G. A. [1988]: *Continuum Mechanics of Electromagnetic Solids*, Vol. 33 of *North-Holland Series in Applied Mathematics and Mechanics.* Elsevier Science Publishers, Amsterdam.

[15] Miehe, C.; Keck, J. [2000]: *Superimposed finite elastic-viscoelastic-plastoelastic stress response with damage in filled rubbery polymers. Experiments, modelling and algorithmic implementation.* Journal of the Mechanics and Physics of Solids, 48(2): 323–365.

[16] Pao, Y.-H.; Hutter, K. [1974]: *A dynamic theory for magnetizable elastic solids with thermal and electrical conduction.* Journal of Elasticity, 4 No.2: 89–114.

[17] Pao, Y.-H.; Hutter, K. [1975]: *Electrodynamics for Moving Elastic Solids and Viscous Fluids*. Proceedings of the IEEE, 63: 1011–1021.

[18] Pelrine, R.; Kornbluh, R.; Joseph, J.; Heydt, R.; Pei, Q.; Chiba, S. [2000]: *High-field deformation of elastomeric dielectrics for actuators*. Materials Science and Engineering: C, 11(2): 89–100.

[19] Plante, J.S.; Dubowsky, S. [2006]: *Large-scale failure modes of dielectric elastomer actuators*. International Journal of Solids and Structures, 43(25-26): 7727–7751.

[20] Plante, J.S.; Dubowsky, S. [2007]: *On the performance mechanisms of dielectric elastomer actuators*. Sensors and Actuators A: Physical, 137(1): 96–109.

[21] Rosato, Daniele [2010]: *On the Formulation and Numerical Implementation of Dissipative Electro Mechanics at Large Strains*. Ph.D. Thesis, Stuttgart University.

[22] Shankar, R.; Ghosh, T.; Spontak, R. [2007]: *Dielectric elastomers as next-generation polymeric actuators*. Soft Matter, 3(9): 1116–1129.

[23] Simo, JC [1987]: *On a fully three-dimensional finite-strain viscoelastic damage model: formulation and computational aspects*. Computer methods in applied mechanics and engineering, 60(2): 153–173.

[24] Steinmetz, T.; Godel, N.; Wimmer, G.; Clemens, M.; Kurz, S.; Bebendorf, M. [2008]: *Efficient Symmetric FEM-BEM Coupled Simulations of Electro-Quasistatic Fields*. Magnetics, IEEE Transactions on, 44(6): 1346–1349.

[25] Wissler, M.; Mazza, E. [2007]: *Electromechanical coupling in dielectric elastomer actuators*. Sensors and Actuators A: Physical, 138(2): 384–393.

[26] Wissler, M.; Mazza, E. [2007]: *Mechanical behavior of an acrylic elastomer used in dielectric elastomer actuators*. Sensors and Actuators A: Physical, 134(2): 494–504.

[27] Zhao, X.; Hong, W.; Suo, Z. [2007]: *Electromechanical hysteresis and coexistent states in dielectric elastomers*. Physical review B, 76(13): 134113.